



Multiple layers of seismic anisotropy and a low-velocity region in the mantle wedge beneath Japan: Evidence from teleseismic receiver functions

Erin A. Wirth and Maureen D. Long

*Department of Geology and Geophysics, Yale University, New Haven, Connecticut 06510, USA
(erin.wirth@yale.edu)*

[1] A complete characterization of seismic anisotropy can yield powerful constraints on mantle flow and deformation. This is particularly important for the mantle wedge above subducting slabs, where the geometry of mantle flow remains poorly understood. We seek to better characterize the geometry and strength of anisotropy in the mantle wedge beneath northeast Honshu and Hokkaido, both of which overlie the subducting Pacific plate. Previous studies indicate that upper mantle anisotropy in the Japan subduction zone is highly complex and exhibits dramatic spatial variations. To provide complementary constraints on the along strike variations in anisotropy, we analyze teleseismic receiver functions from stations of the broadband F-net array using the multitaper correlation receiver function estimator. Backazimuthal variations in P-to-SH converted energy provide clear evidence for complicated anisotropic structure in the mantle wedge beneath northeast Honshu and Hokkaido. In northeast Honshu, forward modeling of receiver functions using synthetic seismograms suggests the presence of an anisotropic layer in the forearc mantle wedge above the subducting slab and a second anisotropic layer beneath the crust of the overriding plate. We also see evidence for a region of low (isotropic) velocity in the central part of the wedge beneath NE Honshu. Comparisons between transverse component receiver functions at stations located in NE Honshu and Hokkaido reveal striking differences, providing further evidence for along strike variation in anisotropic structure in the mantle wedge beneath Japan.

Components: 13,600 words, 15 figures, 2 tables.

Keywords: Japan; receiver functions; seismic anisotropy.

Index Terms: 7240 Seismology: Subduction zones (1207, 1219, 1240).

Received 6 April 2012; **Revised** 25 June 2012; **Accepted** 28 June 2012; **Published** 14 August 2012.

Wirth, E. A., and M. D. Long (2012), Multiple layers of seismic anisotropy and a low-velocity region in the mantle wedge beneath Japan: Evidence from teleseismic receiver functions, *Geochem. Geophys. Geosyst.*, 13, Q08005, doi:10.1029/2012GC004180.

1. Introduction

[2] The mantle wedge above subducting slabs plays an important role in many of the physical processes associated with subduction, yet the geometry of

the flow field in the mantle wedge remains poorly understood. Fortunately, we have the potential to constrain mantle flow and deformation by characterizing the geometry and strength of seismic anisotropy. Anisotropy in the upper mantle appears to be dominated by the lattice preferred orientation



(LPO) of mantle minerals, primarily olivine, resulting from the strain associated with mantle flow [e.g., Silver, 1996; Karato *et al.*, 2008; Long and Becker, 2010]. Consequently, if we can determine the dominant orientation of the olivine fast axes, we can use mineral physics results to deduce the likely direction of mantle flow.

[3] Seismic anisotropy in the subduction zone mantle wedge is most often interrogated by measuring shear wave splitting of local S phases from slab earthquakes. The shear wave splitting parameters (fast polarization direction and delay time) give us information about the orientation of the olivine fast axis (related to the direction of mantle flow) and the strength or extent of the anisotropy, respectively. S-wave splitting is a path-integrated measurement, which means that depth constraints are poor. Additional constraints on anisotropic structure with improved depth resolution can be provided by receiver function analysis. Receiver functions provide information regarding sharp seismic velocity contrasts (both isotropic and anisotropic) beneath a seismic station, and have been used extensively to study crustal structure [e.g., Yamauchi *et al.*, 2003; Ramesh *et al.*, 2005; Abe *et al.*, 2010], the subduction system [e.g., Shiomi *et al.*, 2004; Chen *et al.*, 2005; Tonegawa *et al.*, 2006; Kawakatsu and Watada, 2007], and deep mantle discontinuities [e.g., Li *et al.*, 2000; Niu *et al.*, 2005] beneath Japan. Receiver functions can be used to provide a view of mantle deformation in subduction systems that is complementary to that obtained with shear wave splitting [e.g., Park *et al.*, 2002]. Additionally, in the actively deforming mantle wedge where a simple corner flow model would not generally predict sharp velocity contrasts, any P-to-S conversions that we do see in receiver function analysis must be linked to prominent, well-defined structures.

2. Motivation

[4] A complete characterization of seismic anisotropy is particularly important for understanding the mantle wedge beneath Japan, which overlies multiple subduction zones with complex slab morphologies. Japan's dense seismic instrumentation has enabled many seismological studies, and Japan is perhaps the best-studied subduction system in the world. However, efforts to constrain seismic anisotropy in the mantle wedge beneath Japan have mostly been limited to measurements of shear wave splitting of direct S-waves from events originating in the subducting Pacific and Philippine Sea plates [e.g., Ando *et al.*, 1983; Fouch and Fischer, 1996;

Nakajima and Hasegawa, 2004; Long and van der Hilst, 2006; Nakajima *et al.*, 2006; Salah *et al.*, 2008, 2009; Wirth and Long, 2010; Huang *et al.*, 2011a, 2011b], studies of P wave anisotropy [e.g., Ishise and Oda, 2005; Wang and Zhao, 2008, 2009], and surface wave analysis [e.g., Yoshizawa *et al.*, 2010]. Receiver functions as a tool for characterizing anisotropic structure have mainly been utilized in southwest Japan [i.e., Shiomi and Park, 2008; Nagaya *et al.*, 2011], and have not been thoroughly studied in northeast Japan.

[5] Taken together, previous studies of anisotropic structure beneath Japan reveal two striking first-order findings. One is that mantle wedge anisotropy beneath Japan is highly complex, with strong lateral heterogeneity and abrupt transitions in observed fast directions that often correspond to the volcanic front. A second striking result that has emerged from these studies is the observation of exceptionally small shear wave splitting delay times beneath NE Honshu in comparison to the rest of Japan. Using high frequency energy (2–8 Hz), Nakajima and Hasegawa [2004] measured shear wave splitting delay times ranging from 0.1 to 0.26 s in northwest Honshu and 0.06–0.1 s in northeast Honshu. Using slightly lower frequency energy (0.125–0.5 Hz), Wirth and Long [2010] measured delay times ranging from 0.25 to 0.35 s in NE Honshu. This is significantly smaller than local S splitting measurements made elsewhere in Japan, including Hokkaido (~0.35–1 s at 0.125–0.5 Hz [Wirth and Long, 2010]), the Ryukyu arc (~0.75–1.25 s at 0.02–0.125 Hz [Long and van der Hilst, 2006]), Izu-Bonin (~0.15–1.35 s at 0.1–1 Hz [Fouch and Fischer, 1996]), and central and southwest Honshu (~0.1–1.25 s at 0.01–1 Hz [Salah *et al.*, 2008]). This result implies key differences in the structure of anisotropic fabric beneath NE Honshu and the surrounding regions that must be identified before we can fully understand the mantle flow field.

3. Constraints on Anisotropy From Receiver Function Analysis

[6] When a teleseismic P wave encounters a horizontal velocity discontinuity at depth, it will convert to an SV-wave, arriving at the receiver as an S-wave (termed Ps phase). However, when a ray passes through a dipping interface or anisotropic medium, the scattering of energy will cause an additional SH component of motion, visible on the transverse component waveform [e.g., Levin and Park, 1997; Bostock, 1998; Savage, 1998]. P-to-SH converted energy can also be caused by the scattering



of energy due to small-scale velocity heterogeneities, or topography on the surface or an interface at depth [e.g., *Hu and Menke, 1992; Abers, 1998; Jones and Phinney, 1998*].

[7] There are several characteristics that distinguish Ps conversions due to dipping structure and sharp gradients in anisotropy. In the case of a dipping interface and assuming that bulk velocity increases with depth, Ps conversions from events that are located updip (relative to the dipping structure) will arrive at the seismic station earlier than Ps conversions originating from events in the downdip direction. Therefore, the arrival time of a Ps phase (relative to the P wave) due to dipping structure will vary with the backazimuth (receiver to source direction) of the event, and the character of this variation provides evidence for the strike and dip of the layer. Similarly, the amplitude of the SH energy on the transverse component receiver function also depends on the direction of propagation of the ray, and this variation in SH amplitude with backazimuth contains information about the nature of the interface. In the simplest case, a dipping interface will result in a two-lobed pattern of the Ps phase on the transverse component receiver function gather (that is, two polarity changes within the full backazimuthal range, or a $\sin(\theta)$ pattern, where θ is the backazimuth). In the case of a flat layer, anisotropy with a horizontal symmetry axis will result in a four-lobed polarity flip (or a $\sin(2\theta)$ pattern), although there appear to be other orientations of anisotropy that will result in a four-lobed polarity flip when dipping interfaces are involved (auxiliary material).¹ Energy on the transverse component receiver functions will disappear at backazimuths parallel to the dip of an inclined interface or at backazimuths parallel and orthogonal to a horizontal anisotropic symmetry axis. For anisotropy with a tilted axis of symmetry, the transverse component receiver function will display a mixture of two- and four-lobed patterns. P-SH scattered energy from a shallow point source will also result in a two-lobed polarity flip on the transverse component, but can be distinguished from a dipping interface by an accompanying two-lobed polarity flip on the radial component [*Jones and Phinney, 1998*].

[8] An additional distinction between SH energy due to dipping interfaces and anisotropic structure is the presence or lack of a zero delay arrival (i.e., the direct P arrival) on the transverse component receiver function. Due to the bending of direct P wave energy

out of the source-receiver plane upon encountering a dipping interface, SH motion due to a dipping interface will show a zero delay arrival on transverse component receiver functions, while SH motion due solely to anisotropy will not.

[9] In addition to constraining dipping layers and anisotropic symmetry axes, receiver functions can place certain constraints on structure that are not easily inferred from other methods such as shear wave splitting. For instance, one can determine the depth to contrasts between isotropic or anisotropic layers, the orientation of non-horizontal axes of symmetry, and (through forward modeling) the seismic velocities within each layer.

[10] Here we present P-to-S receiver function analysis on data from seven broadband seismic stations of the F-net network on the islands of Honshu and Hokkaido (Figure 1). Our results are complementary to previous shear wave splitting results [e.g., *Wirth and Long, 2010*], as they provide more precise depth constraints on anisotropic layers and can allow us to determine the orientation of non-horizontal axes of symmetry. Also, direct comparison between receiver functions generated at stations in NE Honshu and stations in Hokkaido will shed light on the differences in anisotropic character in each of these regions that have been elucidated by previous shear wave splitting studies.

4. Data Preprocessing and Methodology

[11] The seismic data used in this study were obtained from Japan's F-net network (www.fnet.bosai.go.jp), a regional array of broadband STS-1 and STS-2 seismometers maintained by Japan's National Institute for Earth Science and Disaster Prevention (NIED). We focus on data from the F-net stations that recorded anomalously short shear wave splitting delay times in NE Honshu and comparable stations to the north in Hokkaido which recorded comparatively longer delay times [*Wirth and Long, 2010*] (Figure 1). All of the stations used in this study are long running, with installation dates before 2004, and therefore we were able to compute receiver functions for 500+ seismic events for most stations. The one exception to this was the shortest running station, TSK, for which 353 events were used. To ensure high-quality P wave arrivals, we restricted our analysis to events of magnitude ≥ 6 at epicentral distances between 25 and 120°.

[12] Our data selection and processing procedures follow those of recent studies that have applied anisotropic receiver function analysis in a subduction

¹Auxiliary materials are available in the HTML. doi:10.1029/2012GC004180.

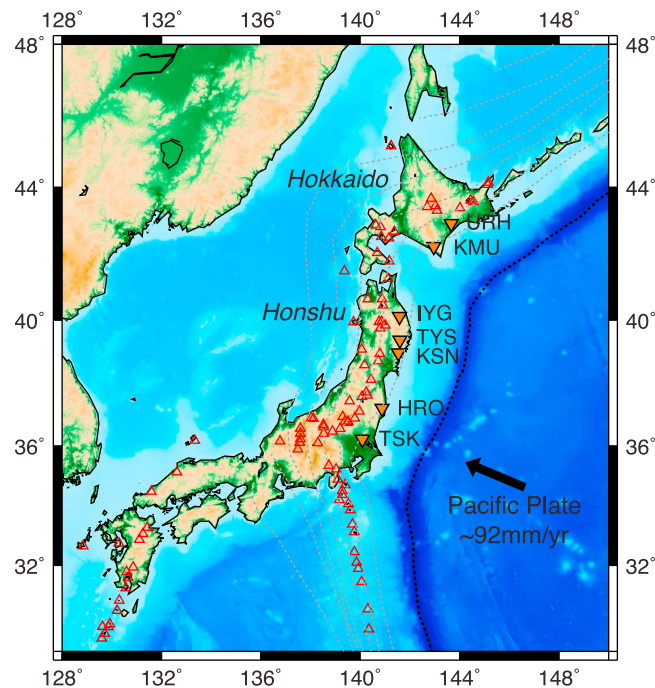


Figure 1. Map showing the topography and tectonic setting of Japan. Black dashed line denotes the location of the Japan trench and slab contours are plotted every 50 km in gray [Syracuse and Abers, 2006]. Red triangles indicate the locations of Holocene volcanoes from the catalog of the Global Volcanism Program (<http://www.volcano.si.edu/world/>) [Siebert and Simkin, 2002]. Inverted orange triangles show the location of the seven F-net stations examined in this study. The black arrow indicates the direction of absolute plate motion for the Pacific plate as given by the HS3-Nuvel1A model [Gripp and Gordon, 2002].

zone setting [Park et al., 2004; Nikulin et al., 2009]. As part of the preprocessing for receiver function analysis, each three-component seismogram was rotated to vertical, radial, and transverse components, and low-pass filtered at 1 Hz. Using the Seismic Analysis Code [Goldstein and Snoke, 2005], we manually select an 80 s time window on each seismogram (beginning at the P wave arrival) that is used for the ensuing analysis. Receiver functions were computed in the frequency domain using the multitaper correlation receiver function estimator, in which receiver functions are computed from the correlation between the vertical component and each of the horizontal components [Park and Levin, 2000]. Receiver functions were then stacked in overlapping 20° intervals with a bin spacing of 10° for both backazimuth and epicentral distance. Individual receiver functions were weighted by their frequency domain uncertainties, with the uncertainty estimated from the coherence between the vertical and horizontal components [Park and Levin, 2000]. We do not correct for moveout due to variations in slowness, and therefore the distribution of the events used (Figure 2) plays an important role in Ps phase moveout and amplitude. The directional dependence of seismic velocity that is indicative of

anisotropy is seen most clearly in the backazimuthal gathers, and therefore we restrict our discussion to these figures.

5. Results and Interpretation

[13] Here we describe the robust features of the receiver function gathers at each station. We divide the stations into three groups based on geographic location: Hokkaido stations (KMU and URH), NE Honshu stations (IYG, TYS, and KSN), and central Honshu stations (HRO and TSK). All stations are located approximately 50–70 km above the Pacific slab (Table 1) [Syracuse and Abers, 2006] and the incidence angles at the surface for incoming direct P waves are approximately 20° or less. Along northeastern Honshu, the Pacific slab is descending at an angle of ~30°, but progressively steepens to ~40° beneath the Hokkaido corner (Table 1) [Syracuse and Abers, 2006]. Therefore, our receiver functions sample a fairly narrow swath of the forearc mantle wedge beneath each station (Figure 3).

[14] We focus the ensuing discussion on those features that are most relevant to this study. Namely, we look for P-to-S conversions and transverse

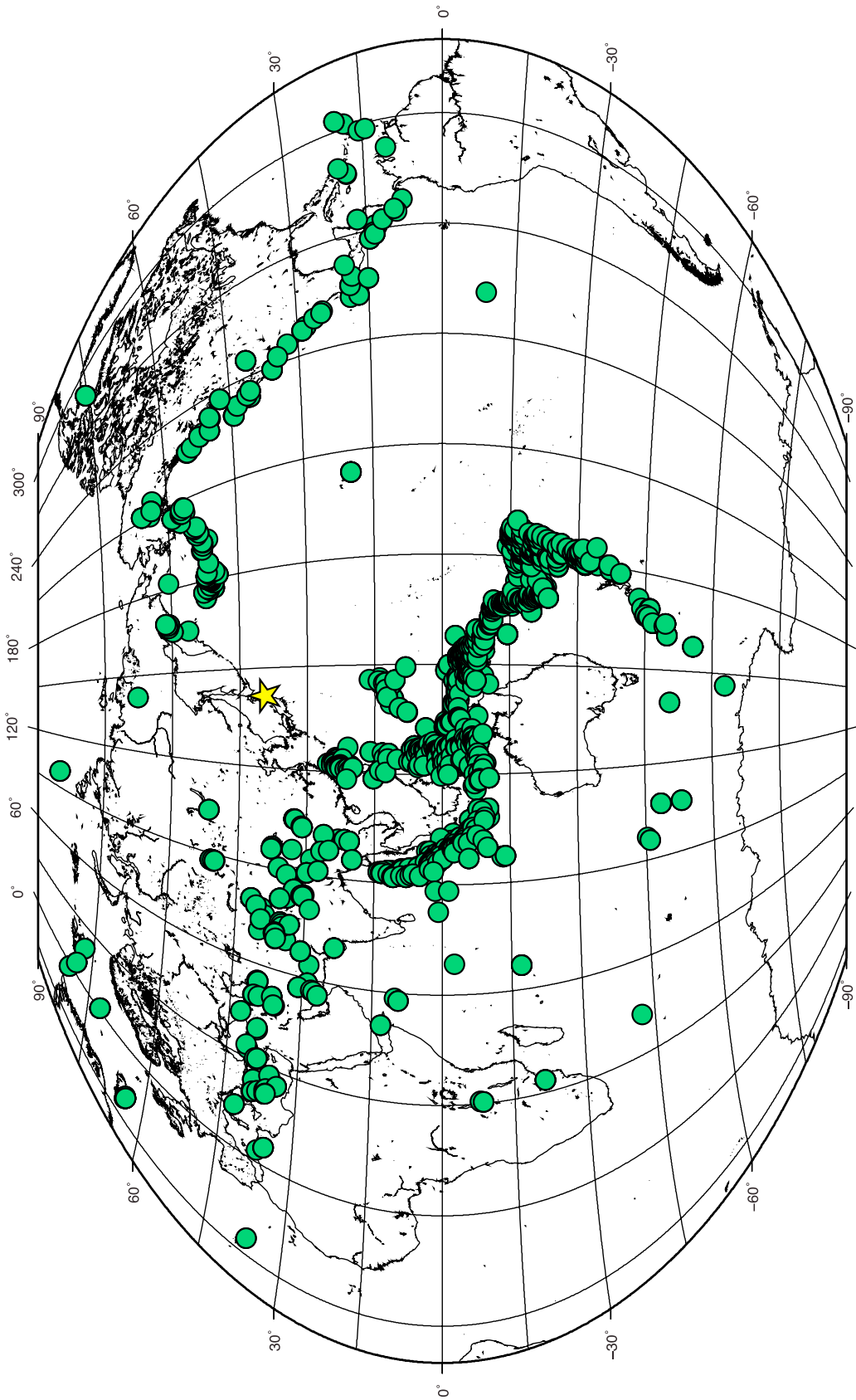


Figure 2. Plot showing the distribution of seismicity (green circles) used in this study. A yellow star in the center of the map denotes our region of study in Japan.

Table 1. The Depth to and Dip of the Slab Beneath Each of Our Stations Based on Work by *Syracuse and Abers* [2006]^a

	Hokkaido			NE Honshu		Central Honshu	
Station	URH	KMU	IYG	TYS	KSN	HRO	TSK
Depth	75 km	45 km	70 km	65 km	65 km	50 km	50 km
Dip	42°	42°	29°	29°	29°	34°	34°

^aThe dip of the slab is based on estimates beneath the volcanic arc.

component polarity flips that are due to structure in the subducting oceanic lithosphere or in the mantle wedge. We do not attempt to analyze the layering or anisotropic structure within the crust of the overriding plate. In general, positive pulses, which are shown in blue, represent a velocity increase with depth. Negative pulses, shown in red, represent a velocity decrease with depth. A time delay of zero corresponds to the direct P wave arrival. A nonzero delay time corresponds to the difference in arrival time between the direct P wave and a Ps phase at the seismic station.

[15] Predicted arrival time times for a Ps conversion at a hypothetical orientation of the slab beneath the station are overlain on all of our receiver function gathers. We use a simple, ray-based method inspired by *Langston* [1977] that accounts for one inclined interface embedded in an isotropic medium. In our model setup, $V_p = 8000$ m/s below the interface,

$V_p = 6900$ m/s above the interface, $V_p/V_s = 1.8$, and the incidence angle of the P wave is set to 20° . The strike, dip, and depth of the layer beneath the seismic station are varied for each station, according to the parameters shown in Table 1.

5.1. Hokkaido

5.1.1. Station URH

[16] Radial component receiver functions at station URH (Figure 4) show a coherent positive pulse at ~ 3 s, indicating a velocity increase with depth. This pulse is likely a result of a P-to-S conversion at the Moho of the overriding plate. We also observe a negative pulse at $\sim 7-9$ s and a positive pulse at $\sim 8-10$ s, both of which are coherent across most backazimuths and display similar variations in the timing of the arrival with backazimuth (moveout patterns). These pulses arrive sooner from events

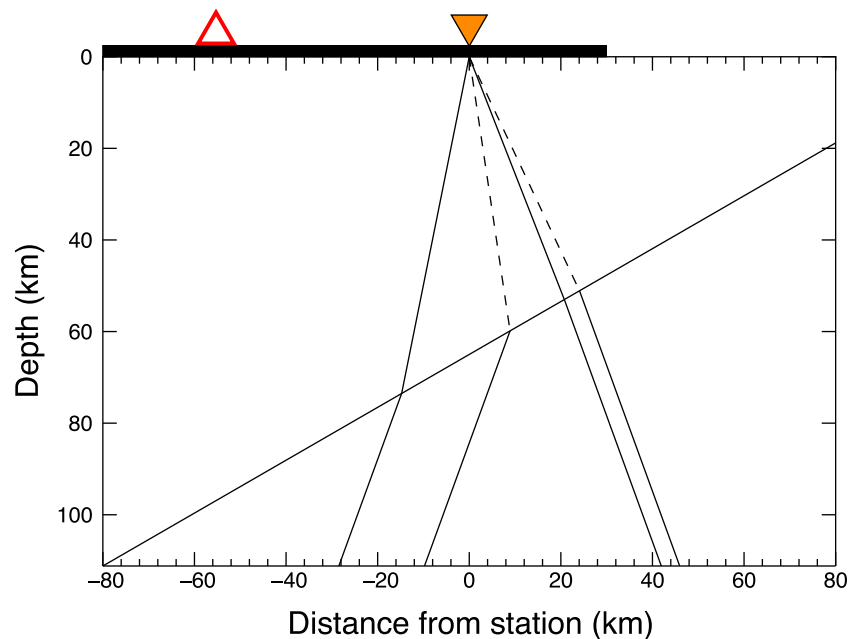


Figure 3. A rough sketch showing the extent of the mantle wedge that is sampled by our station-event geometry. Only those rays that sample farthest from the station are plotted. Solid lines represent P waves and dashed lines represent S-waves. The red triangle marks the approximate location of the volcanic front, and the inverted orange triangle marks the approximate location of the seismic station. The black bar indicates the island of Honshu.

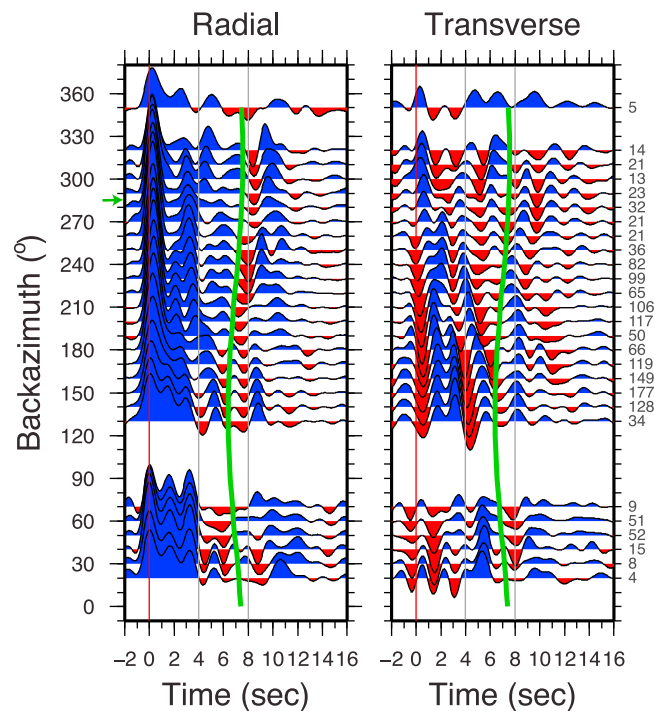


Figure 4. Receiver function results for station URH in Hokkaido. Receiver functions are plotted as a function of time (horizontal axis), with zero being the arrival of the P wave at the seismic station, and grouped by backazimuth (vertical axis). A small green arrow along the vertical axis indicates the downdip direction of the slab. Positive pulses (blue) represent a velocity increase with depth and negative pulses (red) represent a velocity decrease with depth. As a visual aid, gray lines are plotted at 4 and 8 s. The number of receiver functions that are being stacked is indicated to the right of each trace. The thick green line represents the approximate arrival time from a Ps conversion due to a dipping interface that is 70 km below the station, has a strike of 225°, and a 40° dip.

located in the updip direction (that is, arriving from the southeast and a backazimuth of $\sim 135^\circ$), than from events located in the downdip direction (arriving from the northwest and a backazimuth of $\sim 315^\circ$). This timing is consistent with P-to-S conversions at the top of the subducting oceanic crust and at the subducting oceanic Moho, respectively. A positive pulse at ~ 5 – 6 s often precedes this negative-positive pulse doublet, but it is not well defined across all backazimuths. The transverse component receiver functions show a mixture of $\sin(\theta)$ and $\sin(2\theta)$ patterns, which we interpret as being predominantly due to both dipping and anisotropic structure. The coherence of the transverse component phases across all backazimuths, as well as the lack of prominent polarity reversals on the radial component, lead us to conclude that point scatterers in the mantle wedge play a less significant role than dipping structure in creating the $\sin(\theta)$ patterns [Jones and Phinney, 1998]. There is also evidence for energy on the transverse component receiver functions at zero delay time, which is commonly interpreted as evidence for dipping structure. The pattern seen here (a flip from negative to positive at

$\sim 280^\circ$) is indicative of either a westward dipping, fast-over-slow interface or an eastward dipping slow-over-fast interface. We note that this signal may be significantly complicated by near surface structure and scatterers in the shallow crust. Unfortunately, distinct polarity reversals at nonzero delay time on the transverse component are difficult to detect. However, we do see evidence of a polarity reversal at a backazimuth of 240° (roughly trench-parallel) at 6–8 s. By comparing the receiver functions at backazimuths of 70° and 130° , we deduce a likely polarity flip at 6–8 s in the data gap between backazimuths of 80° and 120° , although the limited source distribution prevents us from imaging this feature.

5.1.2. Station KMU

[17] Radial component receiver functions at station KMU show positive pulses at ~ 3 s from backazimuths of 30 – 180° and ~ 2 – 3 s for backazimuths of 190 – 350° (Figure 5). Similar to station URH, this pulse is likely due to a conversion at the Moho of the overriding plate. There is evidence of yet

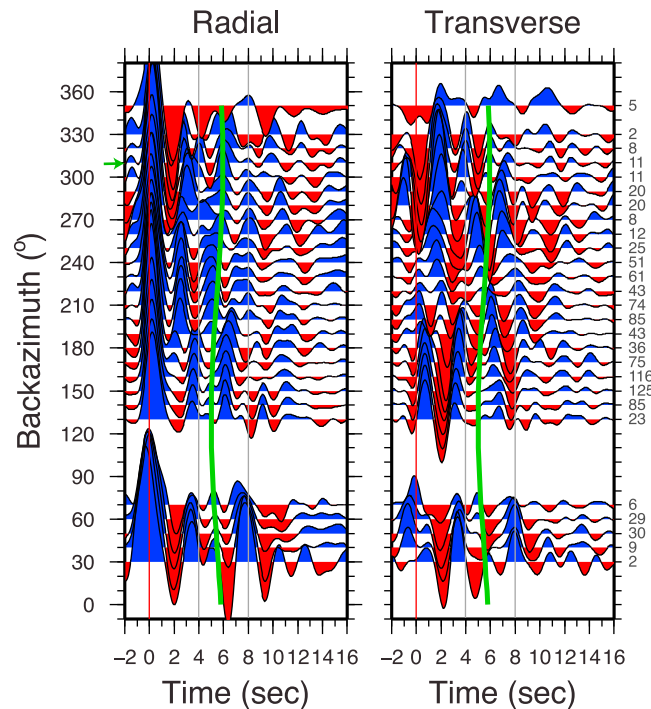


Figure 5. Receiver function results for station KMU in Hokkaido. Receiver functions are plotted as described in Figure 4. The thick green line represents the approximate arrival time from a Ps conversion due to a dipping interface that is 55 km below the station, has a strike of 220° , and a 40° dip.

another positive pulse at $\sim 5\text{--}6$ s, which is most evident at backazimuths greater than $\sim 180^\circ$. At $\sim 6\text{--}8$ s, we see a positive pulse that is coherent across all backazimuths and that has moveout consistent with a conversion at a layer dipping toward a direction of $\sim 290^\circ$. We deduce that this is likely a conversion at the subducting oceanic Moho. There is some evidence of a preceding negative pulse at ~ 6 s, perhaps a conversion at the top of the subducting oceanic crust. The transverse component receiver functions are the most complex of any of the stations analyzed, perhaps a result of stacking relatively fewer receiver functions or due to the complex slab morphology at the Hokkaido corner (Figure 1). An apparent polarity flip at zero delay time between $240^\circ\text{--}290^\circ$ (a flip from positive to negative with increasing backazimuth) is discernable, but is not robust enough for interpretation. The positive zero delay time arrival ($<240^\circ$) is hardly above the noise level (where the noise level is estimated from the size of the pulses coming in earlier than zero delay time), and the receiver functions with the negative zero delay time arrival ($>290^\circ$) have an unusually large amplitude that may be a result of contamination from a few poor traces and stacking relatively few receiver functions. However, we do observe relatively clear polarity reversals occurring at a backazimuth of $\sim 220^\circ$ (again, roughly

trench-parallel) at both ~ 4 s and ~ 6 s. We also infer a likely polarity flip in the data gap between backazimuths of 80° and 120° at ~ 6 s.

5.2. NE Honshu

5.2.1. Station IYG

[18] On the radial component receiver functions at IYG we see a strong pulse at ~ 3 s that is coherent across nearly all backazimuths and is a clear indication of P-to-S conversions at the Moho of the overriding plate (Figure 6). At $\sim 6\text{--}9$ s, we observe the arrival of a negative-positive pulse doublet, which has the appropriate moveout and arrival time for conversions at the subducting oceanic crust and the subducting oceanic Moho, respectively. This doublet is often preceded by another positive pulse at $\sim 5\text{--}7$ s that is seen most clearly at backazimuths of $20\text{--}260^\circ$. Transverse component receiver functions show several instances of polarity reversals, the most prominent of which occurs at $\sim 6\text{--}7$ s at backazimuths of 190° and 260° (roughly trench-parallel and trench-perpendicular, respectively), with a likely additional reversal in the data gap from backazimuths of 70° to 120° . We also see a clear positive-to-negative polarity reversal at zero delay time and a backazimuth of 270° . This is

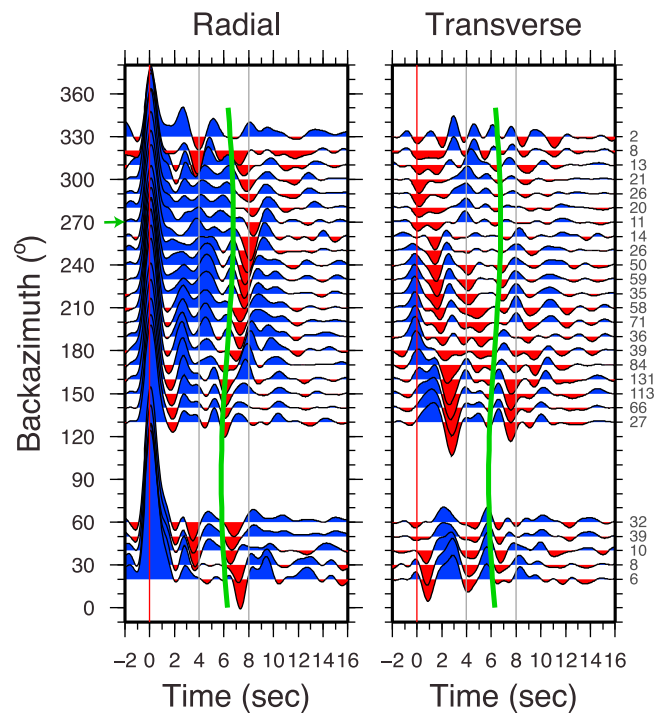


Figure 6. Receiver function results for station IYG in NE Honshu. Receiver functions are plotted as described in Figure 4. The thick green line represents the approximate arrival time from a Ps conversion due to a dipping interface that is 60 km below the station, has a strike of 180° , and a 35° dip.

consistent with a slow-over-fast, westward dipping interface and likely corresponds to the subducting oceanic Moho, which features prominently in the receiver functions from this station.

5.2.2. Station TYS

[19] The radial component receiver functions at station TYS exhibit a coherent positive pulse at ~ 3 s, consistent with a conversion at the Moho of the overriding plate (Figure 7). Some backazimuths (e.g., $200\text{--}260^\circ$) show evidence of an earlier positive pulse at $\sim 1\text{--}2$ s, perhaps due to a mid-crustal discontinuity. A prominent positive-negative-positive series of pulses can be seen at $\sim 5\text{--}9$ s and is coherent across all backazimuthal angles. Based on its moveout and timing, the latter positive pulse is likely the P-to-S conversion at the subducting oceanic Moho and the negative pulse is a conversion at the top of the subducting oceanic crust. The earlier positive pulse seems to indicate a conversion upon entering a layer of comparatively lower velocity. The moveout of this pulse closely follows that of the pulses associated with conversions at the top of the subducting plate, suggesting the lower boundary of this low velocity layer lies parallel to the dip of the slab. The negative pulse that would be associated

with the top of this layer is only clearly visible at backazimuths of 180° to 260° , perhaps suggesting that the upper boundary is not sharply defined. Transverse component receiver functions at TYS show the clearest polarity reversals of all the stations analyzed in this study. The most prominent reversals occur at backazimuths of $\sim 180^\circ$ (trench-parallel) and 280° (trench-perpendicular), at time delays of ~ 6 s. The polarity reversal at $\sim 180^\circ$ does not fit the signal that we would expect to see from a dipping interface in a westward dipping subduction system (i.e., a polarity reversal at the updip, 90° , and downdip, 270° , backazimuths). Therefore, we infer that this particular polarity flip is likely due to another factor, such as seismic anisotropy. Zero delay time arrivals are not significant, although there is some evidence for a negative-to-positive polarity flip at 280° . The amplitudes of these pulses are very low, in contrast to the more robust pulses at adjacent station IYG that showed a positive-to-negative polarity flip at 270° .

5.2.3. Station KSN

[20] Radial component receiver functions at KSN show a positive pulse at $\sim 2\text{--}3$ s that displays some moveout, perhaps indicating a slightly inclined

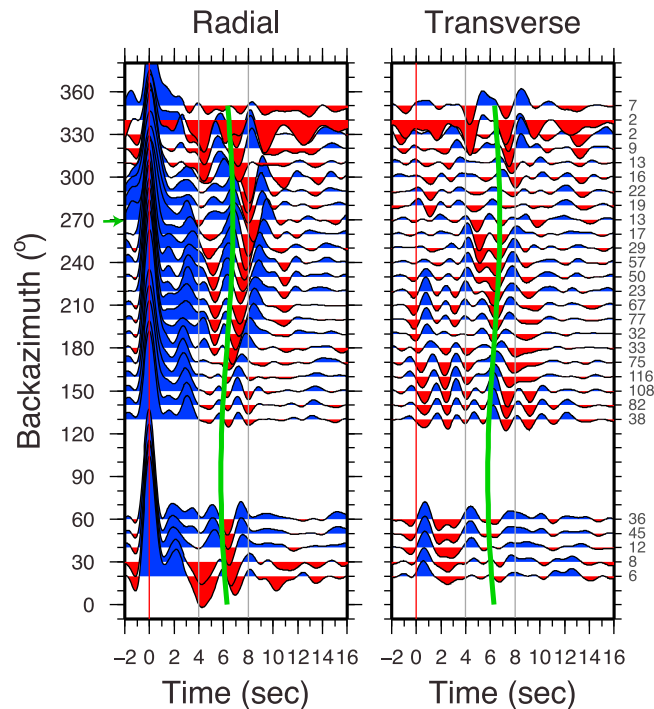


Figure 7. Receiver function results for station TYS in NE Honshu. Receiver functions are plotted as described in Figure 4. The thick green line represents the approximate arrival time from a Ps conversion due to a dipping interface that is 60 km below the station, has a strike of 180° , and a 35° dip.

Moho in the overriding plate (Figure 8). Similar to station TYS, a positive-negative-positive series of pulses is coherent across most backazimuths at ~ 5 – 9 s (with the exception of backazimuths between 20° – 70°), indicative of conversions at the subducting oceanic Moho, the top of the subducting oceanic crust, and perhaps the base of a lower velocity layer. Transverse component receiver functions show polarity reversals at backazimuths of 170° and 200° , at ~ 7 – 8 s and ~ 5 s, respectively. Also at ~ 7 – 8 s, we again infer a likely polarity flip occurring in our data gap (backazimuths of 80° – 120°). Transverse component patterns are quite similar to those seen at station TYS, indicating that the anisotropic structure of the wedge is likely similar. This is perhaps unsurprising given the proximity of the two stations, which are ~ 100 km apart.

5.3. Central Honshu

5.3.1. Station HRO

[21] On the radial component receiver functions at HRO we observe positive pulses arriving at ~ 2 – 4 s delay times from certain backazimuths (20 – 60° , 190 – 350° ; Figure 9). Based on their timing, these P-to-S conversions likely originate at the Moho of

the overriding plate; however, we note that the pulses are not coherent across all backazimuths. A clear negative-positive doublet is visible at ~ 6 – 9 s at all backazimuths, consistent with a conversion at the top of the subducting oceanic crust and the subducting oceanic Moho, respectively. There is also evidence for a positive pulse preceding this doublet at ~ 4 – 5 s, which is clearest at backazimuths of 20 – 170° and 340 – 350° . Transverse component receiver functions reveal fewer coherent features than those from NE Honshu stations; however, we do observe a clear polarity reversal at ~ 6 s from backazimuths of 150° and 240° . We also see a clear polarity flip from positive to negative at zero delay time at a backazimuth of 280° . Again, this is consistent with a slow-over-fast, westward dipping interface.

5.3.2. Station TSK

[22] Radial component receiver functions at TSK exhibit a positive pulse at ~ 3 s that is coherent across all backazimuths and is consistent with a P-to-S conversion at the Moho of the overriding plate (Figure 10). A positive-negative-positive pulse triplet is observed at ~ 6 – 9 s from backazimuths in the range of 170 – 260° . This is a negative-positive

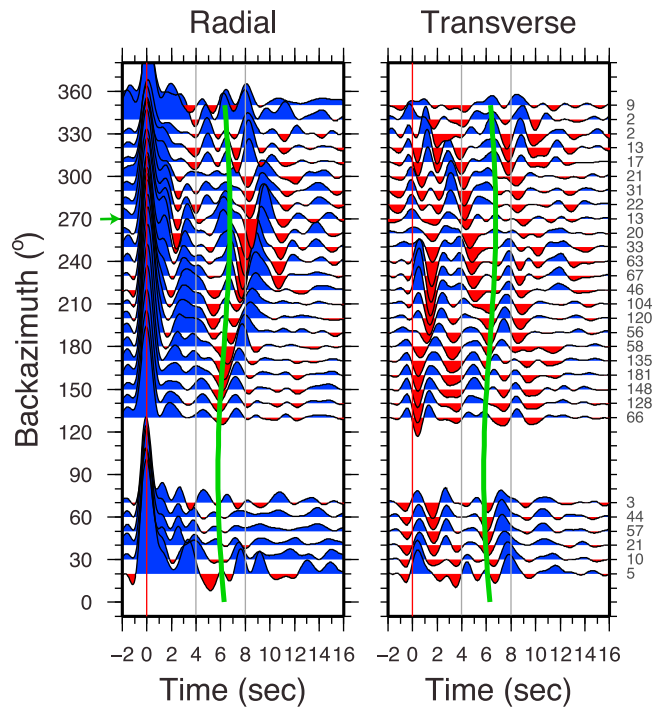


Figure 8. Receiver function results for station KSN in NE Honshu. Receiver functions are plotted as described in Figure 4. The thick green line represents the approximate arrival time from a Ps conversion due to a dipping interface that is 60 km below the station, has a strike of 180° , and a 35° dip.

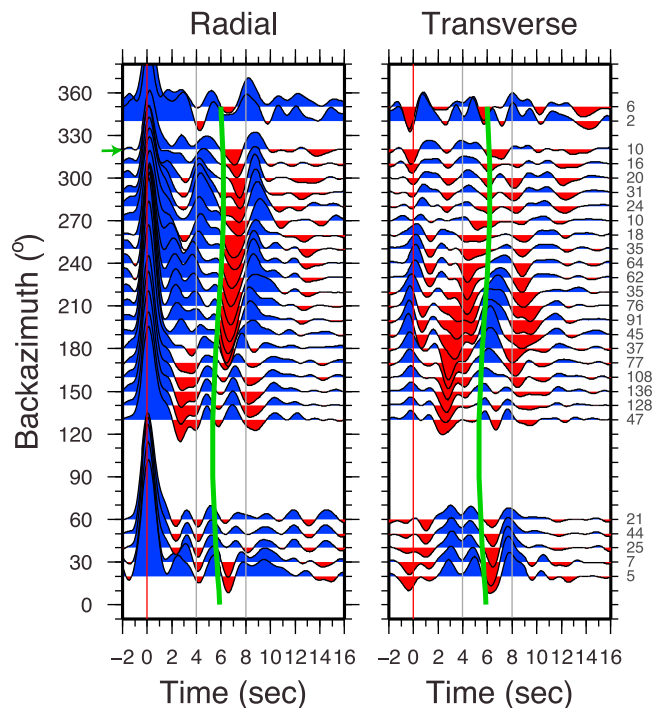


Figure 9. Receiver function results for station HRO in central Honshu. Receiver functions are plotted as described in Figure 4. The thick green line represents the approximate arrival time from a Ps conversion due to a dipping interface that is 55 km below the station, has a strike of 200° , and a 35° dip.

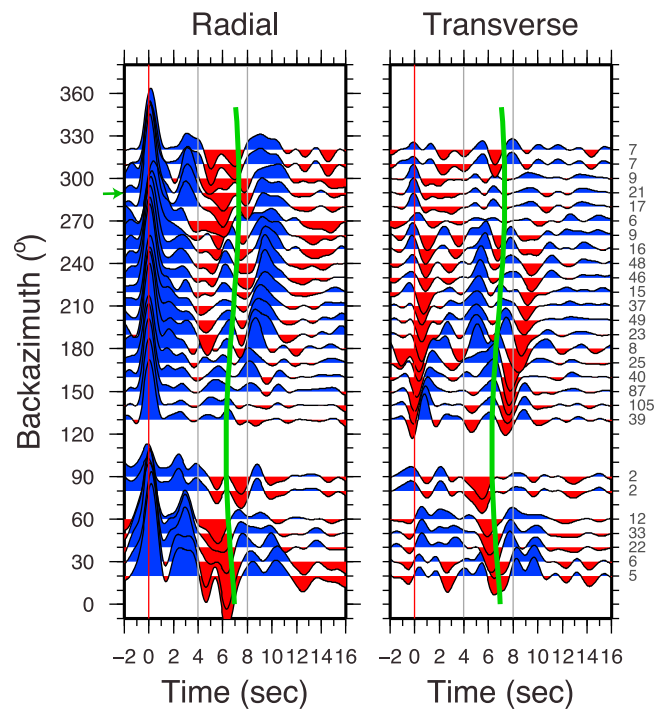


Figure 10. Receiver function results for station TSK in central Honshu. Receiver functions are plotted as described in Figure 4. The thick green line represents the approximate arrival time from a Ps conversion due to a dipping interface that is 65 km below the station, has a strike of 200° , and a 35° dip.

pulse doublet at all other backazimuths, a result of conversions at the top of the subducting oceanic crust and slab Moho, respectively. Transverse component receiver functions are complex, but exhibit polarity reversals at backazimuths of 180° and 260° , at time delays of ~ 6 – 8 s. Zero delay time arrivals are complex, and inconsistent with the signal we would expect to see from east-west dipping interfaces (polarity reversals at 90° or 270°). As has been noted for previous stations, this is likely due to localized shallow structure that results in complicated P-to-SH scattered energy.

5.4. Summary and Comparison

[23] To bolster confidence in our results and interpretation, we emphasize the prominence of the conversions from three well-established structures: the overriding plate Moho, the top of the subducting oceanic crust, and the Moho of the subducting plate. The crustal thickness in northeast Honshu is roughly ~ 30 – 35 km [e.g., Taira, 2001]. Assuming $V_P = 6.2$ km/s and $V_P/V_S = 1.72$, a crustal thickness of 30 km, and a vertical incidence angle, Ps conversions from the overriding plate Moho should arrive roughly 3.5 s after the P wave, as is true for all of our northeast Honshu stations. The moveout and absolute arrival time of the P-to-S conversions

associated with the slab are consistent with a westward dipping interface at 50–70 km depth, which matches the known characteristics of the Pacific slab beneath our stations. The coherence of the pulses associated with these three features lend confidence to our methods and also clearly bound the range of Ps arrival times where we would expect to see conversions from structure within the mantle wedge. We also examined receiver functions gathered by epicentral distance (as opposed to backazimuth) in order to ensure that the pulses we are interpreting are not multiples from shallow interfaces, such as PpP phases [Savage *et al.*, 2007]. Examples of these epicentral distance gathers are shown in the auxiliary material.

[24] A comparison of our data with results from previous studies also supports the notion that we are seeing real Ps conversions. Past receiver functions studies [i.e., Chen *et al.*, 2005; Tonegawa *et al.*, 2006] have imaged both the subducting oceanic Moho and the top of the subducting oceanic crust in NE Honshu at the same approximate depths (down to ~ 130 km) and with a dip angle of $\sim 30^\circ$. The overriding plate Moho was imaged at 25–40 km depths. Kawakatsu and Watada [2007] also used receiver functions to detect the subducting oceanic Moho, whose signal they find dissipates between

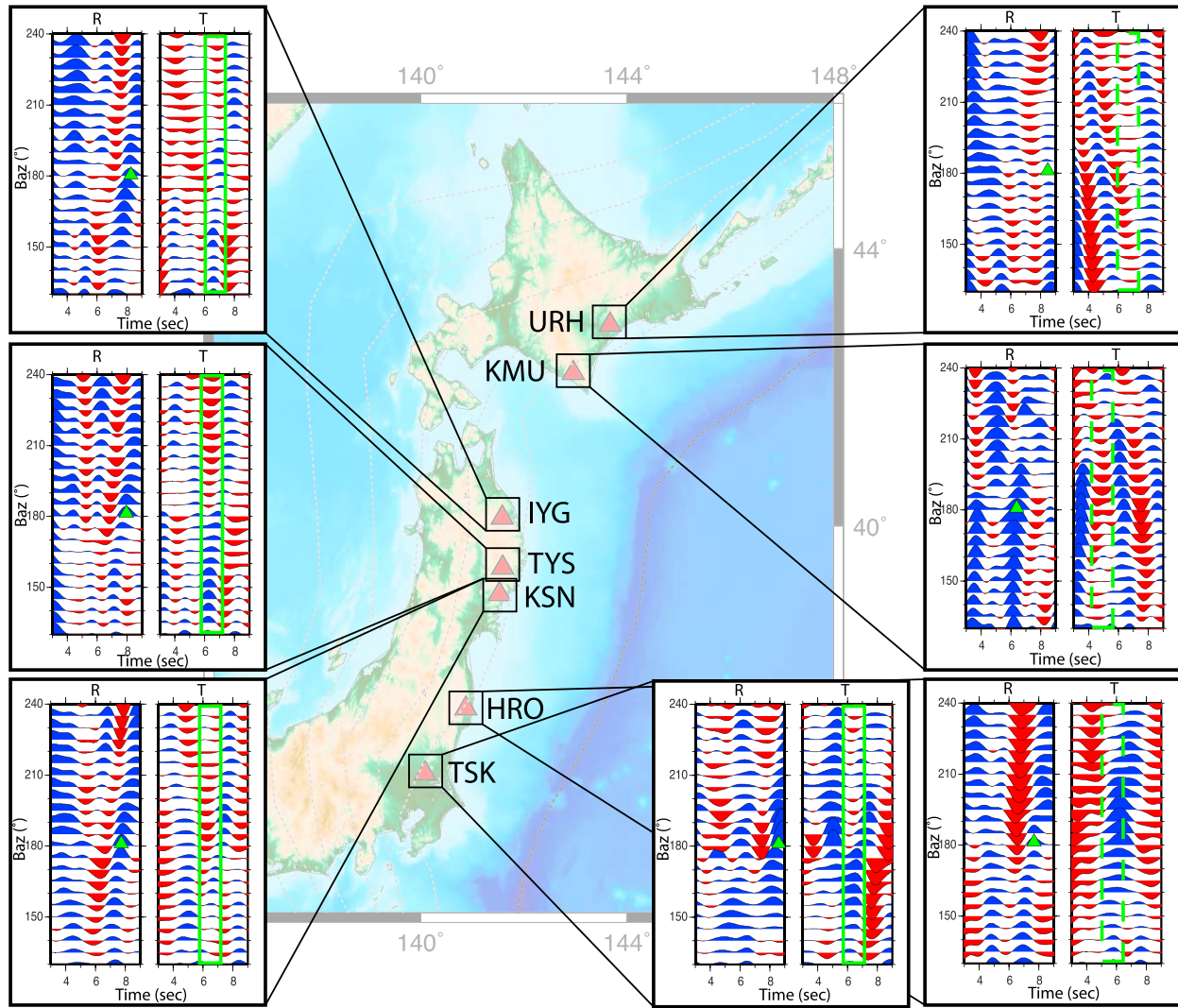


Figure 11. Receiver function results for all stations from a select group of backazimuths, focusing on a narrow time window where we would expect to see Ps conversions from structure in the mantle wedge. Black lines connect each receiver function gather with the corresponding station where the data was recorded. For reference, green triangles on the radial component indicate the positive pulse associated with the subducting oceanic Moho. On the transverse component, we place a green box around the time window associated with structure immediately above the subducting slab. Three stations from NE Honshu and one station from central Honshu exhibit a clear polarity flip $\sim 180^\circ$ (solid green box), while stations in Hokkaido do not (dashed green box).

50 and 90 km depths due the dehydration of the subducting oceanic crust, which results in a decreasing velocity contrast between the ocean crust and adjacent overriding mantle. In our study, the slab is approximately 50–70 km beneath each station (Table 1), and therefore still within the range where we would expect to see some signal from a conversion at the subducting oceanic Moho based on their results.

[25] A comparison of our radial and transverse component receiver function gathers (Figure 11)

among groups of stations and, in some cases, between adjacent stations, reveals striking lateral variations in mantle wedge structure beneath Japan. The two Hokkaido stations have receiver functions that are not only visually distinct from receiver functions computed elsewhere in Japan, but also from each other. The Ps signal from the Moho of the subducting plate arrives significantly later for station URH ($\sim 8\text{--}10$ s) than for station KMU ($\sim 6\text{--}8$ s). This difference corresponds well to the difference in estimated depth to the slab beneath each station (~ 70 km and ~ 50 km, respectively

[Syracuse and Abers, 2006]). Unlike at station URH, radial component receiver functions from station KMU are highly complex and do not show a strong signal from a conversion at the top of the subducting oceanic crust. For both stations, it is difficult to clearly delineate the backazimuths at which transverse component polarity reversals occur. Yet, even a cursory visual inspection reveals that the transverse components at station URH and KMU are quite different (Figures 4 and 5). We attribute the variation between these two closely spaced stations to the tectonic complexity of the Hokkaido corner [e.g., Miller *et al.*, 2006], as well as differences in the depth to the slab beneath each station.

[26] Receiver functions computed at NE Honshu stations IYG, TYS, and KSN exhibit many similar features that allow us to regard them as a coherent group. Nearly all of the radial component receiver functions exhibit a positive-negative-positive pulse triplet at $\sim 5\text{--}9$ s, which we interpret as conversions at the subducting oceanic Moho, the top of the subducting oceanic crust, and an apparent low velocity region in the mantle wedge. All transverse component receiver functions for Honshu stations except HRO show a polarity reversal at $\sim 180^\circ$ ($\pm 15^\circ$) at $\sim 5\text{--}8$ s (Figure 11). Stations TYS and KSN also show polarity reversals at $\sim 200\text{--}210^\circ$ at ~ 5 s.

[27] Receiver functions from central Honshu stations HRO and TSK are unfortunately not as coherent as those computed for NE Honshu stations. There is some evidence of a positive-negative-positive pulse triplet on the radial components at $\sim 4\text{--}9$ s, but this signal is not coherent across all backazimuths. Similar to NE Honshu stations, station TSK (Figure 10) shows evidence of a transverse component polarity reversal at $\sim 180^\circ$ and $\sim 260^\circ$ at ~ 6 s. This is slightly different than station HRO (Figure 9), where we see some evidence for polarity reversals at $\sim 150^\circ$ and $\sim 240^\circ$ backazimuths at ~ 6 s. To first order, receiver functions from central Honshu stations have more features in common with those computed for NE Honshu stations than Hokkaido stations.

6. Mantle Wedge Structure From Forward Modeling of Receiver Functions

6.1. Forward Modeling of Receiver Functions: Approach and Methodology

[28] The visual inspection of the major features of our receiver function gathers and the qualitative

comparisons among different stations described above can place first-order constraints on the seismic structure of the mantle wedge beneath Japan. More precise and quantitative constraints on this structure can be obtained through forward modeling of receiver functions. By comparing synthetic receiver functions to receiver functions generated by actual data, we can determine how well a given model represents Earth structure. We generated synthetic seismograms using ANIREC, a flat-layer reflectivity algorithm [Levin and Park, 1997], and RAYSUM, a code for creating ray theoretical seismograms in the presence of dipping interfaces [Frederiksen and Bostock, 2000]. We make the simplifying assumption of hexagonally symmetric anisotropy, which allows us to fully describe the orientation of anisotropy using just two parameters (azimuth and dip of the symmetry axis). The parameters used to define the input model include the number of layers and (for each layer in the model) the layer thickness, density, V_P , V_S , percent anisotropy (if any), trend and plunge of the anisotropic symmetry axis, whether it is a fast or slow axis of symmetry, and, for RAYSUM, the strike and dip of the interface. Once the synthetic seismograms are generated using these model parameters, we compute their receiver functions using the multitaper correlation receiver function estimator and using the same procedure that was used on the actual data.

[29] It may appear that a 1-D flat-layer model such as the one used in the ANIREC algorithm might not be ideal for describing a subduction zone setting. However, previous studies have successfully used flat-layer reflectivity algorithms to model mantle wedge structure in Cascadia [e.g., Park *et al.*, 2004; Nikulin *et al.*, 2009]. We do note that the slab dip in Cascadia ($\sim 10^\circ$) is shallower than in northeast Honshu ($\sim 30^\circ$). Yet, one advantage of the ANIREC program is that it utilizes the backazimuths and epicentral distances from a collection of real data. This way, the station-event geometry (and therefore, incidence angles) between the synthetic receiver functions and actual receiver functions are consistent, and it allows for a more accurate representation of Ps phase amplitudes. Wave propagation codes such as RAYSUM that incorporate both anisotropy and dipping structure are available and are obviously better suited for subduction zone settings [e.g., Frederiksen and Bostock, 2000]. However, because of the extra parameters involved (strike and dip of each layer), they are much more difficult to use to match real data without the help of a model space search. In addition, the RAYSUM code uses one representative slowness value (we use

6E-2 s/km) for each backazimuthal angle and does not take into account the actual event-station geometry, making it difficult to match the Ps amplitudes and moveout for the real data correctly.

[30] While our forward models contain a large number of free parameters that describe several seismic properties, we emphasize that the results for the orientation of the anisotropic symmetry axis and/or dipping layers are often the most reliable. Tradeoffs exist between layer thickness and (isotropic) P- and S- wave velocities; increasing layer thickness has the same effect on Ps delay time as decreasing V_S or increasing V_P . As previously discussed, polarity reversals will occur on the transverse component receiver function at backazimuths that are parallel or perpendicular to the symmetry axis in the case of anisotropy, and parallel to the dip of the layer in the case of inclined structure. These characteristic patterns are unaffected by isotropic seismic wave speed or layer thickness and can be clearly seen in the original receiver functions.

6.2. Application to Station TYS

[31] We have focused on deriving a model for Earth structure beneath station TYS in NE Honshu because of the clear, coherent features observed on both the radial and transverse receiver function gathers. In particular, the clear polarity reversals and multitude of strong, coherent pulses observed on the transverse components across all backazimuths should allow us to place strong constraints on the anisotropic geometry. Receiver functions from TYS exhibit many similarities to those computed at other stations (e.g., IYG and KSN; see Figures 6–8), and therefore the results of forward modeling can be applied broadly to the NE Honshu region.

[32] We began with the ANIREC forward modeling code, and an isotropic velocity starting model based on P and S-wave travel time data from local events [Nakajima *et al.*, 2001], making small alterations to the seismic velocities to more accurately match the arrival time of Ps phases from our data. We also took into account in our starting model the location of the subducting Pacific slab at depth [Syracuse and Abers, 2006]. Since the ANIREC code does not allow for dipping layers, pulses on our synthetic receiver functions do not exhibit any moveout with backazimuth, but the moveouts observed in the actual data are completely consistent with a dipping slab.

[33] Most pulses on the radial component were easily matched by accounting for known discontinuities that are likely to be present in a subduction zone (the

Moho of the overriding plate, the top of the subducting oceanic crust, and the Moho of the subducting plate). However, in order to reproduce the positive pulse observed on the radial component TYS receiver functions at ~ 6 s, a region of low velocity was required at 35–50 km depth. Varying the V_P/V_S ratio within this layer did not significantly alter the synthetic receiver functions. If we choose not to interpret the negative pulse at ~ 5 s in our TYS receiver functions as a P-to-S conversion upon exiting this low velocity layer (mainly because this pulse is not coherent across all backazimuths), then the mantle wedge layer above the low velocity region is not required.

[34] After matching the main features of the radial component receiver functions with an isotropic model, we began to add anisotropy to our working model to match the most robust features on the transverse component. Due to the large number of free parameters in the forward modeling, our approach to identifying models that fit the transverse receiver function data mainly relied on trial and error. However, we tested a large range of anisotropic geometries and strengths to be sure that the model presented here represents a global best fit to the data. We first tried to match the four-lobed polarity flip on the transverse component receiver functions at ~ 6 s (Figure 12, purple square and blue triangle). We successfully replicated this pattern by adding an anisotropic layer between 50 and 60 km depths (down to the top of the subducting oceanic crust), that has 5% anisotropy and a fast symmetry axis oriented trench-perpendicular (i.e., toward a direction of 270°). A slow axis that is trench-parallel (i.e., oriented toward 180°) gives the same result. The strength (percent) of the anisotropy is constrained based on the amplitudes of the transverse component pulses. This appears to be accurate to within a few percent, but we note that the amplitude of the pulses may change significantly with the inclusion of dipping interfaces. We also tried adding anisotropy into the subducting oceanic crust to see if it provides a better match to the actual data. We found that the addition of 3% anisotropy in the downgoing slab crust with a trench-perpendicular slow axis dipping 30° from horizontal results in subtle improvements on the transverse component receiver functions. More specifically, the synthetic pulses exhibit a slight broadening at backazimuths from 20 to 60° and 130 – 180° at ~ 8 s that is consistent with the actual data (Figure 12, green circle). However, it is not entirely clear if this pulse is actually broadening, or if it is simply merging with the adjacent red negative pulse at ~ 9 s. Finally, we

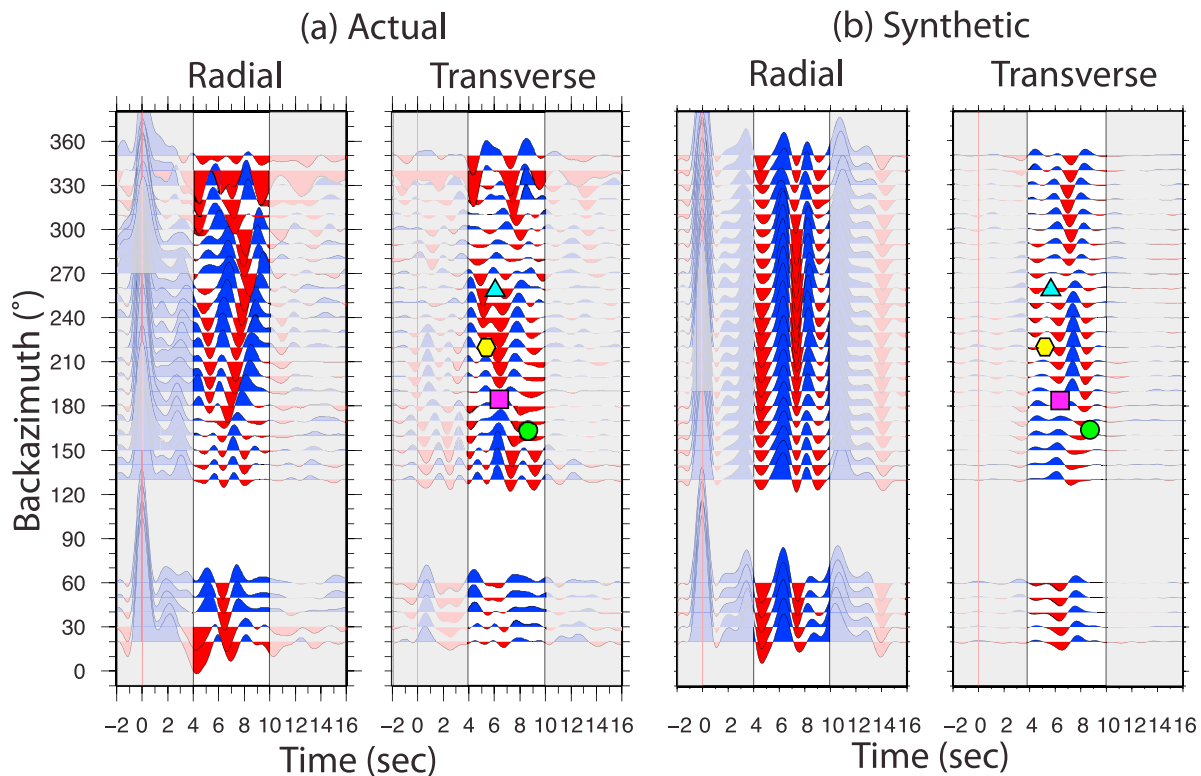


Figure 12. Receiver functions computed for station TYS using (a) actual data and (b) synthetic seismograms generated by the ANIREC code and the model parameters given in Table 2. Receiver functions are plotted as described in Figure 4. We focus on matching the features at 4–10 s (unshaded). Colored symbols denote features on the transverse component that we were able to replicate particularly well with our synthetic model (see section 6.2).

also sought to replicate the observed polarity flip at a backazimuth of 220° at ~ 5 s. In a layer between 25 and 35 km depth, we prescribed 3% anisotropy with a horizontal fast axis of symmetry oriented at an azimuth of 220° . This matches the observed polarity flip (Figure 12, yellow hexagon) but does not result in any other improvements to the data fit.

[35] Our final best fitting model of the seismic structure of the mantle wedge beneath station TYS using ANIREC is shown as a cartoon sketch in Figure 13 and the model parameters are given in Table 2. To summarize, the most salient features of this model in terms of seismic anisotropy (and implications for mantle flow and deformation) are 1) a 10 km thick anisotropic layer directly beneath the crust of the overriding plate, which has 3% anisotropy and a fast direction roughly parallel to the direction of Pacific plate subduction, 2) a 10 km thick anisotropic layer directly above the slab, with a fast direction that parallels the downdip motion of the plate, and 3) the anisotropic crustal layer in the downgoing slab, which has 3% anisotropy with a slow axis of symmetry that is tilted slightly

downward (30° in our model) with respect to the dip of the downgoing slab.

[36] We repeated the forward modeling process using the RAYSUM code, which can include dipping interfaces, to generate synthetic seismograms. First, to ensure consistency between the two forward modeling approaches, we input the flat layer model that was a “best fit” with the ANIREC code into RAYSUM. The resulting receiver function predictions match well in Ps arrival time and polarity, but not in transverse component amplitude (auxiliary material). ANIREC tends to produce larger amplitude Ps phases on the transverse component for a given percent anisotropy than does RAYSUM. Again, this variation in amplitude may be due to the fact that ANIREC takes into account the actual station-event geometry of the data set. This variation is not a major issue in our modeling approach, as our emphasis is on the orientation of anisotropy, not necessarily its strength.

[37] We again take the best fit model determined by ANIREC and input it into RAYSUM, but this time including dipping interfaces where we believe them to be appropriate (i.e., the subducting oceanic

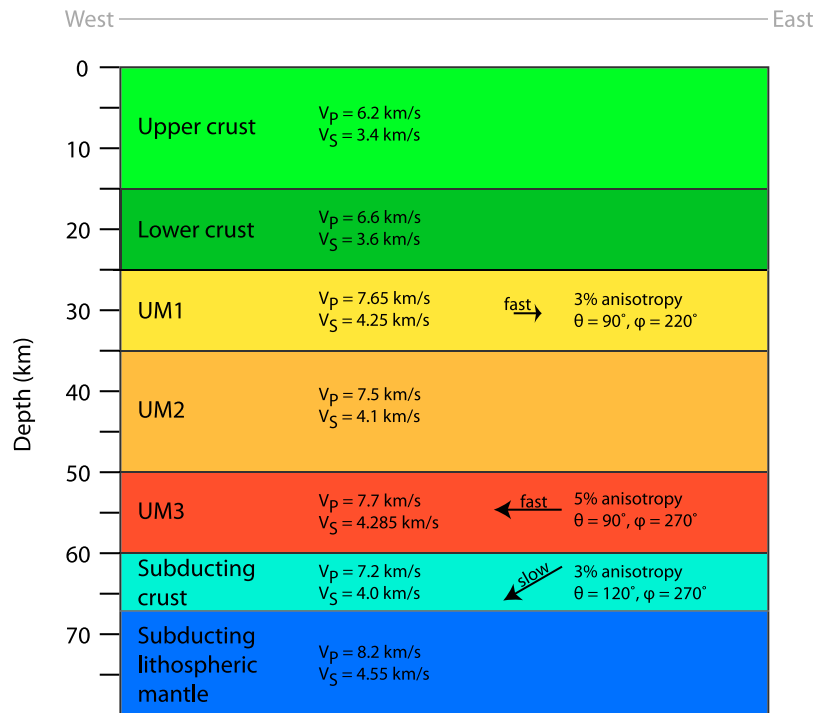


Figure 13. Sketch of the model of Earth structure beneath station TYS in NE Honshu used to create the synthetic receiver functions shown in Figure 12 using the ANIREC code. All of the model parameters are also given in Table 2.

Moho, the top of the subducting oceanic crust, and a layer immediately above the slab, all of which show the appropriate moveout for dipping structure in our actual receiver function data). Each layer

retains its anisotropic signature, but the symmetry axes are rotated such that they are still oriented the same relative to the layer interfaces (i.e., a horizontal layer with a horizontal axis of symmetry in

Table 2. Model Parameters Used to Generate the Synthetic Receiver Functions Shown in Figures 12 and 14^a

Depth (m)	V_p (m/s)	V_s (m/s)	ρ (g/cm ³)	% Anisotropy	θ (°)	ϕ (°)	Strike (°)	Dip (°)
<i>ANIREC Best Fit</i>								
15000	6200	3400	2600	—	—	—	—	—
25000	6600	3600	2900	—	—	—	—	—
35000	7650	4250	3250	3	90	220	—	—
50000	7500	4100	3200	—	—	—	—	—
60000	7700	4285	3300	5	90	270	—	—
67000	7200	4000	3000	−3	120	270	—	—
	8200	4550	3300	—	—	—	—	—
<i>RAYSUM Best Fit</i>								
15000	6200	3400	2600	—	—	—	—	—
25000	6600	3600	2900	—	—	—	—	—
35000	7650	4250	3250	3	60	0	—	—
55000	7500	4100	3200	—	—	—	180	30
70000	7900	4400	3300	8	120	90	180	30
77000	7200	4000	3000	—	—	—	180	30
	8200	4550	3300	—	—	—	180	30

^aModel sketches are shown in Figures 13 and 15. Each row corresponds to a different layer in the model. “Depth” refers to the depth to the bottom of the layer from the surface, “ θ ” corresponds to the tilt from vertical of the anisotropic symmetry axis, “ ϕ ” is the azimuth from north of the anisotropic symmetry axis, “strike” refers to the strike of the layer’s upper interface relative to north, and “dip” refers to its dip. A positive percent anisotropy represents a fast axis of symmetry, while a negative percent anisotropy indicates a slow axis of symmetry. Depth refers to the depth of the bottom of the layer. θ = tilt from vertical of anisotropic symmetry axis. ϕ = azimuth from north of anisotropic symmetry axis. Strike refers to the layer’s upper interface, relative to north. Dip refers to the layer’s upper interface, downwards from horizontal.

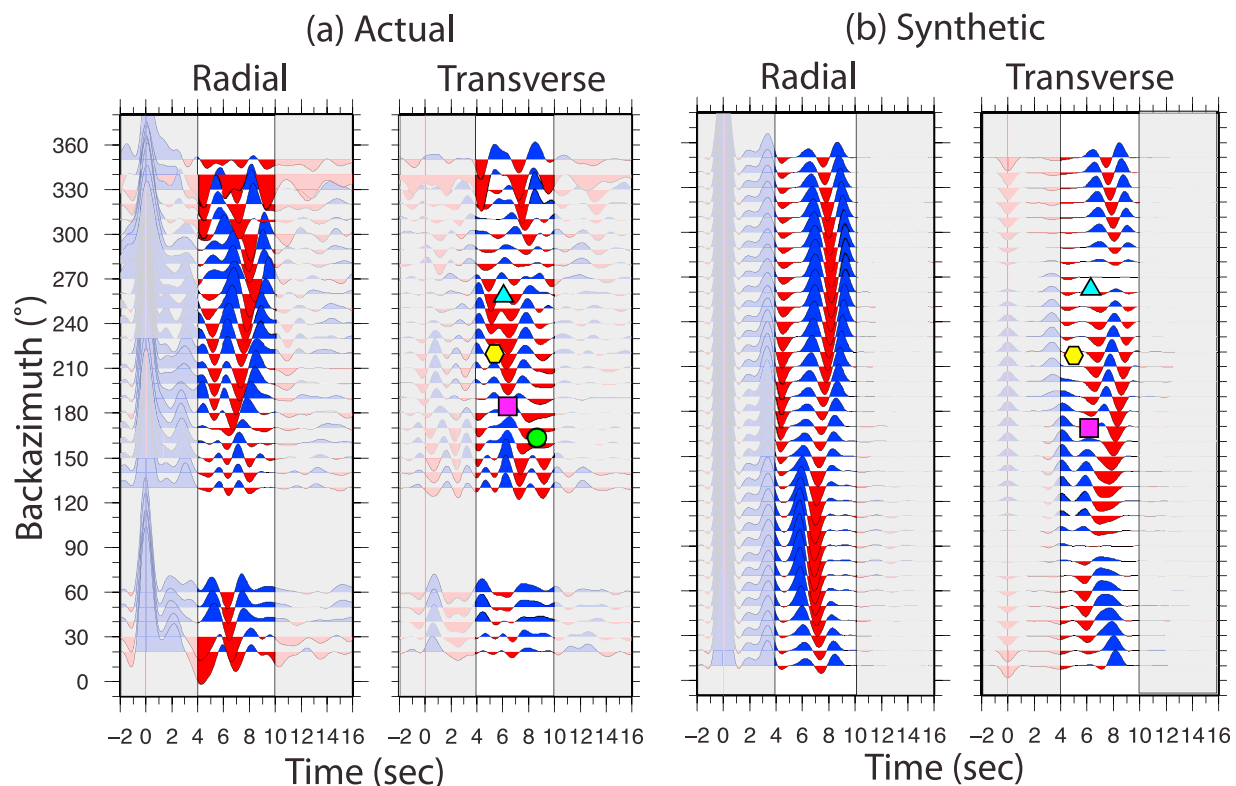


Figure 14. Receiver functions computed for station TYS using (a) actual data and (b) synthetic seismograms generated by the RAYSUM code and the model parameters given in Table 2. Receiver functions are plotted as described in Figure 4. We focus on matching the features at 4–10 s (unshaded). Colored symbols denote features on the transverse component that we were able to replicate particularly well with our synthetic model (see section 6.2).

ANIREC would now be a layer with a 30° dip and an axis of symmetry parallel to the layer interface, also a 30° dip). While this first attempt at creating a best fit model using RAYSUM matched the radial component of our actual data, it does not match our transverse component data well (auxiliary material). This leads us to identify a new best fit model for Earth structure beneath TYS using the RAYSUM code.

[38] Even with a purely isotropic model in RAYSUM, we are able to match some of the transverse component patterns in our data simply by adding dipping structure. A two-lobed polarity reversal at ~ 8 s is easily replicated with the presence of a dipping subducting oceanic Moho. To replicate other significant features, we find it necessary to add anisotropic structure. We find that the four-lobed polarity flip is best matched by an anisotropic 20 km thick layer above the subducting slab, with an axis of symmetry that is dipping at 30° , but in the opposite direction of the slab (Figure 14, purple square). We attempt other orientations that we would also expect to yield a four-lobed polarity flip (auxiliary material),

but do not obtain a good match. We also try orientations that would be expected for B-type olivine fabric (trench-parallel fast axis [Jung and Karato, 2001]) or serpentinite (a slow axis of symmetry perpendicular to the plane of the slab [Katayama *et al.*, 2009]), but these do not provide overall good fits to the data. Finally, to match the negative doublet at ~ 6 s and a backazimuth of 240° in the transverse component, as well as the emerging positive pulse at 270° , we find that a symmetry axis that is trench-parallel but plunging 30° below horizontal provides the best fit (Figure 14, yellow hexagon and blue triangle). Including anisotropy in the subducting oceanic crust did not significantly improve the fit to the data. Our best-fitting model for seismic structure in the mantle wedge beneath station TYS using RAYSUM is shown in a cartoon sketch in Figure 15 and the model parameters are given in Table 2. To summarize, the relevant anisotropic layers in the RAYSUM best fit model are 1) a 20 km thick layer above the slab with a fast axis of symmetry that is parallel to the convergence direction, but plunging 30° eastward, and 2) a 10 km thick layer of anisotropy beneath the crust of the

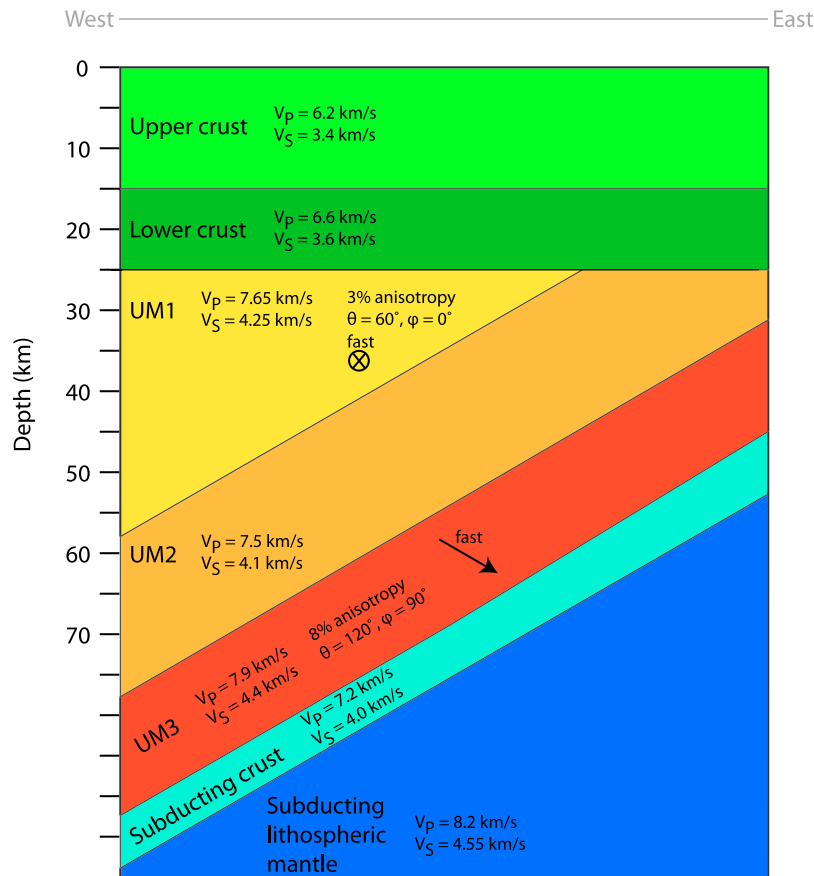


Figure 15. Sketch of the model of Earth structure beneath station TYS in NE Honshu used to create the synthetic receiver functions shown in Figure 14 using the RAYSUM code. Model parameters are given in Table 2.

overriding plate, with a fast axis of symmetry that is trench-parallel and plunging 30° southward.

7. Discussion

7.1. Lateral Variations in Mantle Wedge Structure Beneath NE Honshu and Hokkaido

[39] The most fundamental result from our receiver function analysis is the striking difference among receiver functions computed at Hokkaido stations (URH and KMU) and those computed at stations on the island of Honshu (on both components, but particularly the transverse). Here we discuss the implications of these differences for mantle structure and processes in the mantle wedge beneath the northeastern Japan subduction zone.

[40] We begin by examining differences on the radial component. While all stations show a strong conversion at the subducting oceanic Moho and at the top of the subducting oceanic crust whose

timing corresponds well to the known slab position, NE Honshu stations also exhibit a well-defined Ps phase originating above the subducting slab (i.e., arriving at earlier delay times than the slab conversions), which closely follows the moveout of Ps conversions from the slab. For Hokkaido stations, this Ps phase is not as robust in that it is not well defined, not coherent across all backazimuths, and does not follow the moveout of the slab pulse. Our forward modeling suggests that this phase is due to the contrast between the anisotropic layer directly above the subducting slab and an isotropic low velocity layer in the central part of the mantle wedge beneath NE Honshu stations. The receiver function data at the Hokkaido stations do not show strong evidence for such a low velocity layer, although they do not rule it out.

[41] On the transverse component, NE Honshu stations exhibit a four-lobed polarity flip at ~ 6 s (with the “flips” occurring at backazimuths of $\sim 180^\circ$ and $\sim 280^\circ$) associated with an anisotropic layer directly above the subducting slab (i.e., a Ps



arrival time earlier than the slab conversions but later than conversions from the low velocity layer proposed above) with a symmetry axis parallel to the (dipping) slab. We also note that P-to-S conversions arriving at earlier delay times (~ 3 s or less), associated with shallower structure within the crust of the overriding plate, also have polarity flips at approximately the same backazimuths. This implies that there are several anisotropic structures in the subduction system that have a geometry related to (and likely controlled by) the direction of Pacific plate convergence.

[42] In contrast, the Hokkaido stations show a completely different (and more complicated) pattern of coherent pulses on the transverse component receiver function gathers. We see no evidence of simple four-lobed polarity flips on the transverse components. At station URH in particular (Figure 4), the strength and coherency of the transverse component pulses from ~ 1 – 6 s is quite remarkable. The lack of simple two- or four-lobed polarity flips implies the presence of both dipping layers and complex anisotropic structures with tilted symmetry axes in the mantle wedge. While our model for anisotropic structure beneath NE Honshu is fairly simple, we surmise that the mantle wedge beneath Hokkaido has much more complicated anisotropic structure. The strong, coherent arrivals on the transverse component receiver functions imply that strong gradients in anisotropy are involved, but the geometry of the symmetry axes is likely complex. It is therefore difficult to interpret with our simple flat-layer forward modeling approach. Further modeling work that takes into account more complex anisotropic scenarios, possibly involving a model space search approach that provides a thorough exploration of the large parameter space [e.g., Porter *et al.*, 2011], may be able to identify a physical model for wedge structure beneath Hokkaido that is consistent with our observations.

7.2. Evidence for Dipping Structure in the Mantle Wedge

[43] We see several pieces of evidence for dipping structure associated with the subducting slab in our receiver functions. The most obvious support for the presence of dipping structure is the radial component receiver function moveout patterns. P waves coming from events located in the updip direction (i.e., a backazimuth of 90° for a westward dipping interface, such as the slab beneath Japan) will encounter the interface at shallower depths than P waves originating from events located downdip.

Ps phases that encounter the dipping interface at shallower depths will spend less time as an S-wave, and arrive closer in time to the direct P wave arrival. This results in a sinusoidal pattern of arrival time versus backazimuth that is seen in all of our receiver function gathers. Phases that we interpret as being conversions at the top of the subducting oceanic crust and the subducting oceanic Moho, match well with our estimated arrival times for conversions occurring at a dipping interface with the same depth and orientation as the slab (Figures 4–10, green curves).

[44] A dipping interface will also result in a two-lobed polarity flip of the Ps phase on the transverse component receiver function gather. Energy on the transverse component receiver function will disappear at backazimuths parallel to the dip of the inclined interface. Therefore, for a westward dipping interface and increasing velocity with depth (i.e., the subducting oceanic Moho), Ps phases coming from events originating north of the subduction system should have a positive transverse component polarity, while events coming from the south should have a negative polarity. This matches well with the transverse component polarities that are roughly ~ 1 s later than our predicted arrival curves (Figures 4–10).

[45] As previously mentioned, another indication of dipping structure is a zero delay time arrival on the transverse component receiver function, due to the bending of direct P wave energy out of the source-receiver plane upon encountering a dipping interface. The zero time lag arrivals will be opposite in polarity to the later arriving two-lobed polarity flipped arrival and will not have the associated moveout. Therefore, for a westward dipping slow-over-fast interface, we would expect a negative polarity at zero delay time for events originating north of the subduction system and a positive polarity at zero time delay for events originating south of the subduction system. This particular pattern at zero time lag is most clearly seen at stations IYG (northeast Japan, Figure 6) and HRO (central Japan, Figure 9). Many of the other stations have evidence of zero time lag arrivals that are either of the opposite polarity, or only have energy at zero time delay at certain backazimuths. This is likely due to the effects of near surface scattering or shallow dipping interfaces in the crust that are not parallel to the dip of the slab.

[46] Finally, as the epicentral distance of the source relative to the receiver increases, we expect the incidence angle of the arrival to decrease (i.e.,

become more vertically incident). A vertically incident wave will take a more direct path to the receiver, arriving at the receiver closer to the direct P wave arrival than a ray with a shallow incidence angle. Epicentral gathers of our receiver function data match this expected moveout pattern (auxiliary material).

7.3. Implications of Our Model for Anisotropy in the Mantle Wedge Beneath NE Honshu

[47] The interpretation of our model for Earth structure beneath NE Honshu first requires some discussion regarding the different olivine fabric types. Mineral physics studies have shown that the development of olivine LPO (and therefore the prevalent direction of the olivine fast axes) is sensitive to variability in deformation conditions, including stress, temperature, water content, and perhaps pressure [e.g., *Karato et al.*, 2008]. Relatively dry conditions with moderate stresses and temperatures, as likely in the lithosphere, are conducive to the development of A-type olivine fabric. As water content is increased, mimicking conditions that we may expect in the asthenosphere, E- or C-type fabric becomes dominant. In high stress, low temperature environments with moderate water content, such as the shallow corner of the mantle wedge, mineral physics results suggest the presence of B-type olivine fabric [e.g., *Jung and Karato*, 2001]. The presence of B-type olivine fabric in the mantle wedge is of particular importance because unlike A-, E-, or C-type fabrics for which the olivine fast axes align parallel to the shear direction, in the case of B-type olivine fabric the olivine fast axes align perpendicular to the shear direction.

[48] Serpentinite minerals formed by the hydration of the mantle wedge are also anisotropic, and thus the LPO of serpentinite is a viable candidate mechanism for anisotropy in the shallow, relatively cold corner of the mantle wedge [e.g., *Kneller et al.*, 2008] and directly above the slab [e.g., *Katayama et al.*, 2009], where temperatures are likely within the serpentinite stability field [e.g., *Ulmer and Trommsdorff*, 1995]. However, our model for Earth structure beneath NE Honshu does not require any of the striking geophysical properties commonly associated with serpentinites, such as low seismic velocities [*Christensen*, 1996], a high Poisson's ratio [*Watanabe et al.*, 2007], or very strong anisotropy (single crystal S-wave anisotropy up to ~38% [*Kern*, 1993]). Therefore, we conclude that

the inferred anisotropy beneath NE Honshu is likely caused by the LPO of olivine.

[49] The best fit models for Earth structure beneath station TYS based on the ANIREC and RAYSUM forward modeling codes are not in complete agreement. However, they do agree in several areas: (1) an anisotropic layer directly above the slab is required to match the four-lobed polarity flip on the transverse component receiver functions, (2) a region of lower velocity is required to match the positive pulse on the radial component that precedes the conversions from the slab but appears to have a similar moveout pattern, and (3) there is likely an anisotropic layer directly beneath the crust of the overriding plate. Where the two methods differ is in the estimate of the strength of anisotropy, the thickness of the layers, and the precise orientation of the anisotropic symmetry axis. Since the thickness of the anisotropic layer and the strength of anisotropy are affected by tradeoffs with velocity and our estimates of the Ps phase amplitude (which ANIREC and RAYSUM predict differently), in our interpretation we place the most emphasis on the orientation of the anisotropic symmetry axis.

[50] Although the best fit models for ANIREC and RAYSUM predict somewhat different orientations of the anisotropic symmetry axis, some general conclusions can be drawn. First, the layer of anisotropy above the slab has an axis of symmetry that is either parallel or oblique to the dip of the slab. The models that had trench-parallel fast directions in this layer (as would be consistent with B-type olivine fabric) or a slow axis of symmetry perpendicular to the slab (as would be consistent with serpentinite) did not provide an overall good fit to the data. This leads us to conclude that the fabric above the slab at this depth (~60–70 km) is likely A-, E-, or C-type olivine fabric, with mantle flow that is dictated by the convergence direction. However, we do note that especially in synthetics generated using RAYSUM, P-SH conversions from dipping structure and anisotropic layers appear to interact heavily, and we cannot rule out the possibility that more complicated models may exist that would allow for other orientations of the anisotropic symmetry axes. Identifying such a complex model would require more sophisticated forward modeling techniques, such as a model space search, and is beyond the scope of this study.

[51] The ANIREC and RAYSUM best fitting models disagree more significantly on the orientation of the anisotropic symmetry axis in the layer beneath the crust of the overriding plate. The

ANIREC model predicts a trench-perpendicular axis of symmetry (consistent with A-, C-, or E-type olivine fabric and simple 2-D corner flow), while the RAYSUM model predicts a trench-parallel axis of symmetry that is plunging 30° below horizontal. This orientation is more consistent with B-type olivine fabric and 2-D corner flow or along strike flow and A-, C-, or E-type fabric.

[52] This ambiguity in fast direction orientation is unsurprising given the results of prior studies. Previous studies have proposed that B-type olivine fabric may be present in the shallow corner of the mantle wedge beneath NE Honshu [Nakajima and Hasegawa, 2004; Karato *et al.*, 2008] and invoke this mechanism to explain the transition from trench-parallel fast directions close to the trench to trench-perpendicular fast directions farther into the backarc. However, the very small delay times (0.1 s or less) documented at forearc stations by Nakajima and Hasegawa [2004] do not unambiguously require mantle wedge anisotropy, and may instead reflect crustal anisotropy due to LPO of crustal minerals [e.g., Babuska and Cara, 1991; Levin and Park, 1998], aligned cracks in the shallow crust [e.g., Crampin, 1994], or a combination of these. A recent study by Huang *et al.* [2011a] that attempted to place direct observational constraints on crust, wedge, and slab anisotropy beneath NE Honshu provides some support for this hypothesis. P wave anisotropy studies in the mantle wedge beneath NE Honshu have also yielded inconsistent results, with some studies documenting trench-perpendicular fast directions in the mantle wedge, with trench-parallel fast directions in the subducting slab [i.e., Ishise and Oda, 2005] and others citing the presence of trench-parallel fast directions in the forearc mantle wedge itself [e.g., Wang and Zhao, 2008]. Studies of shear wave splitting and P wave anisotropy in the mantle wedge beneath Hokkaido have also suggested trench-parallel fast directions close to the trench and trench-perpendicular fast directions farther away from the trench, although the orientations appear highly complex [Nakajima *et al.*, 2006; Wang and Zhao, 2009].

[53] Despite these ambiguities, we emphasize that our model is consistent with the observation that NE Honshu has substantially smaller local S shear wave splitting delay times compared to elsewhere in Japan [Wirth and Long, 2010] and subduction zones worldwide [Long and Silver, 2008]. Our models agree on the presence of two anisotropic layers in the mantle wedge, but each is thin (20 km or less) with relatively weak anisotropy (~3–8%), and the total delay time that would be accrued by a

shear wave propagating through our model would be small (~0.2–0.4 s). This is consistent with the ~0.3 s shear wave splitting delay times at these stations observed by Wirth and Long [2010] using direct S-waves from events originating in the subducting Pacific plate.

[54] Our model using ANIREC also contains a layer of anisotropy within the subducting oceanic crust, although the addition of this anisotropy only slightly improves the fit to actual data. We found that a slow axis of symmetry with an east-west orientation and that is inclined slightly relative to the layer interfaces provides the best match. This is consistent with models that invoke anisotropy due to aligned serpentinite filled cracks in the shallow part of subducting slabs [e.g., Faccenda *et al.*, 2008; Healy *et al.*, 2009]. We note, however, that the layer in our model, which has 3% anisotropy in a 7 km thick layer, would predict a splitting delay time less than ~0.1 s, much smaller than global SKS splitting delay times. Adding anisotropy to the subducting oceanic crust in the RAYSUM best fit model did not affect the fit to the actual data.

7.4. A Low Velocity Region Parallel to the Dip of the Slab?

[55] One interesting isotropic feature in our model is the region of relatively low seismic velocities in the central part of the mantle wedge that is present in both the ANIREC and RAYSUM best fit models. This region is necessary in order to reproduce the positive pulse occurring at ~6 s on several of our radial component receiver functions, particularly those in NE Honshu. A low velocity zone that is parallel to the slab has been well documented in NE Honshu using seismic tomography, and is commonly attributed to the presence of partial melt beneath the arc [e.g., Nakajima *et al.*, 2005; Zhao *et al.*, 2009]. This low velocity layer typically extends from the volcanic arc into the backarc, and our stations are located in the forearc region of the mantle wedge. However, tomographic images from these studies do show evidence of low S-wave velocity and low Poisson's ratio areas in small regions of the forearc, adjacent to the arc volcanoes, and at approximately the same depth and geographic location where we infer a low velocity layer. Receiver functions have recently been used to reveal the presence of a somewhat similar low velocity region above the subducting slab in Kamchatka [Nikulin *et al.*, 2012]. However, further petrologic study would be required before any direct comparisons could be made between the NE Honshu low

velocity zone and that in Kamchatka, which is attributed by *Nikulin et al.* [2012] to a secondary melt source in the central part of the wedge. The presence of sediments has also been proposed to explain low velocity layers above the subducting slab [e.g., *Savage et al.*, 2007], but if this were the case, we may also expect to see anisotropy with a slow axis of symmetry, which neither of our models requires.

8. Summary

[56] We have presented a new data set of teleseismic P wave receiver functions for seven seismic stations in Honshu and Hokkaido that allows us to draw several conclusions about the seismic structure of the mantle wedge beneath Japan. First, we find significant evidence for along strike variation in mantle wedge structure beneath NE Honshu and Hokkaido. First order characteristics of transverse component receiver functions, which mainly reflect contrasts in anisotropic structure at depth, are substantially different between stations in NE Honshu and stations in Hokkaido. We see evidence for a low velocity region in the central part of the mantle wedge beneath NE Honshu, but the evidence for a similar layer beneath Hokkaido stations is ambiguous. Second, our forward modeling of receiver functions confirms the likely presence of an anisotropic layer above the slab in NE Honshu, with ~5–8% anisotropy and an anisotropic fast axis that is parallel or oblique to the dip of the down-going slab. Although there is ample evidence for anisotropy in the mantle wedge beneath Hokkaido, we do not see any suggestion of such a clearly defined layer, with a relatively simple orientation of anisotropy, directly above the slab. Finally, our models also suggest an anisotropic layer beneath the crust of the overriding plate in NE Honshu. However, the models disagree as to the orientation of the anisotropic symmetry axis, leaving some ambiguity as to the layer's structure and the origin of its anisotropy.

Acknowledgments

[57] We acknowledge support from NSF grant EAR-0911286 awarded to MDL and an NSF Graduate Research Fellowship awarded to EAW. All data were obtained from the F-net seismic network, which is operated and maintained by the Japanese National Research Institute for Earth Science and Disaster Prevention. All maps and receiver function images were created using the GMT software package [*Wessel and Smith*, 1991]. We are grateful to Vadim Levin and Jeffrey Park for assistance with codes and helpful comments on an early draft of this paper. We

would also like to thank Martha Savage and an anonymous reviewer for their helpful suggestions that greatly improved this paper.

References

- Abe, Y., T. Ohkura, T. Shibutani, K. Hirahara, and M. Kato (2010), Crustal structure beneath Aso Caldera, Southwest Japan, as derived from receiver function analysis, *J. Volcanol. Geotherm. Res.*, *195*, 1–12, doi:10.1016/j.jvolgeores.2010.05.011.
- Abers, G. A. (1998), Array measurements of phases used in receiver function calculations: Importance of scattering, *Bull. Seismol. Soc. Am.*, *88*, 313–318.
- Ando, M., Y. Ishikawa, and F. Yamazaki (1983), Shear wave polarization anisotropy in the upper mantle beneath Honshu, Japan, *J. Geophys. Res.*, *88*, 5850–5864, doi:10.1029/JB088iB07p05850.
- Babuska, V., and M. Cara (1991), *Seismic Anisotropy in the Earth*, Kluwer Acad., Dordrecht, Netherlands, doi:10.1007/978-94-011-3600-6.
- Bostock, M. G. (1998), Mantle stratigraphy and evolution of the Slave province, *J. Geophys. Res.*, *103*, 21,183–21,200, doi:10.1029/98JB01069.
- Chen, L., L. Wen, and T. Zheng (2005), A wave equation migration method for receiver function imaging: 2. Application to the Japan subduction zone, *J. Geophys. Res.*, *110*, B11310, doi:10.1029/2005JB003666.
- Christensen, N. I. (1996), Poisson's ratio and crustal seismology, *J. Geophys. Res.*, *101*, 3139–3156, doi:10.1029/95JB03446.
- Crampin, S. (1994), The fracture criticality of crustal rocks, *Geophys. J. Int.*, *118*, 428–438, doi:10.1111/j.1365-246X.1994.tb03974.x.
- Faccenda, M., L. Burlini, T. V. Gerya, and D. Mainprice (2008), Fault-induced seismic anisotropy by hydration in subducting oceanic plates, *Nature*, *455*, 1097–1100, doi:10.1038/nature07376.
- Fouch, M. J., and K. M. Fischer (1996), Mantle anisotropy beneath northwest Pacific subduction zones, *J. Geophys. Res.*, *101*, 15,987–16,002, doi:10.1029/96JB00881.
- Frederiksen, A. W., and M. G. Bostock (2000), Modelling teleseismic waves in dipping anisotropic structures, *Geophys. J. Int.*, *141*, 401–412, doi:10.1046/j.1365-246x.2000.00090.x.
- Goldstein, P., and A. Snoke (2005), *SAC Availability for the IRIS Community, Inc. Inst. Seismol. Data Manage. Cent. Electron. Newsl.*, *7*, 1–6.
- Gripp, A. E., and R. G. Gordon (2002), Young tracks of hot spots and current plate velocities, *Geophys. J. Int.*, *150*, 321–361, doi:10.1046/j.1365-246X.2002.01627.x.
- Healy, D., S. M. Reddy, N. E. Timms, E. M. Gray, and A. V. Brovarone (2009), Trench-parallel fast axes of seismic anisotropy due to fluid-filled cracks in subducting slabs, *Earth Planet. Sci. Lett.*, *283*, 75–86.
- Hu, G., and W. Menke (1992), Formal inversion of laterally heterogeneous velocity structure from P wave polarization data, *Geophys. J. Int.*, *110*, 63–69, doi:10.1111/j.1365-246X.1992.tb00713.x.
- Huang, Z., D. Zhao, and L. Wang (2011a), Shear wave anisotropy in the crust, mantle wedge, and subducting Pacific slab under northeast Japan, *Geochem. Geophys. Geosyst.*, *12*, Q01002, doi:10.1029/2010GC003343.
- Huang, Z., D. Zhao, and L. Wang (2011b), Frequency-dependent shear-wave splitting and multilayer anisotropy



- in northeast Japan, *Geophys. Res. Lett.*, **38**, L08302, doi:10.1029/2011GL046804.
- Ishise, M., and H. Oda (2005), Three-dimensional structure of P wave anisotropy beneath the Tohoku district, northeast Japan, *J. Geophys. Res.*, **110**, B07304, doi:10.1029/2004JB003599.
- Jones, C. H., and R. A. Phinney (1998), Seismic structure of the lithosphere from teleseismic converted arrivals observed at small arrays in the southern Sierra Nevada and vicinity, California, *J. Geophys. Res.*, **103**, 10,065–10,090, doi:10.1029/97JB03540.
- Jung, H., and S.-I. Karato (2001), Water-induced fabric transitions in olivine, *Science*, **293**, 1460–1463, doi:10.1126/science.1062235.
- Karato, S., H. Jung, I. Katayama, and P. Skemer (2008), Geodynamic significance of seismic anisotropy of the upper mantle: New insights from laboratory studies, *Annu. Rev. Earth Planet. Sci.*, **36**, 59–95, doi:10.1146/annurev.earth.36.031207.124120.
- Katayama, I., K.-I. Hirauchi, K. Michibayashi, and J.-I. Ando (2009), Trench-parallel anisotropy produced by serpentine deformation in the hydrated mantle wedge, *Nature*, **461**, 1114–1117, doi:10.1038/nature08513.
- Kawakatsu, H., and S. Watada (2007), Seismic evidence for deep-water transportation in the mantle, *Science*, **316**, 1468–1471, doi:10.1126/science.1140855.
- Kern, H. (1993), P- and S-wave anisotropy and shear-wave splitting at pressure and temperature in possible mantle rocks and their relation to the rock fabric, *Phys. Earth Planet. Inter.*, **78**, 245–256, doi:10.1016/0031-9201(93)90159-7.
- Kneller, E. A., M. D. Long, and P. E. van Keken (2008), Olivine fabric transitions and shear-wave anisotropy in the Ryukyu subduction system, *Earth Planet. Sci. Lett.*, **268**, 268–282, doi:10.1016/j.epsl.2008.01.004.
- Langston, C. A. (1977), The effect of planar dipping structure on source and receiver responses for constant ray parameter, *Bull. Seismol. Soc. Am.*, **67**, 1029–1050.
- Levin, V., and J. Park (1997), P-SH conversions in a flat-layered medium with anisotropy of arbitrary orientation, *Geophys. J. Int.*, **131**, 253–266, doi:10.1111/j.1365-246X.1997.tb01220.x.
- Levin, V., and J. Park (1998), P-SH conversions in layered media with hexagonally symmetric anisotropy: A Cookbook, *Pure Appl. Geophys.*, **151**, 669–697, doi:10.1007/s000240050136.
- Li, X., S. V. Sobolev, R. Kind, X. Yuan, and C. Estabrook (2000), A detailed receiver function image of the upper mantle discontinuities in the Japan subduction zone, *Earth Planet. Sci. Lett.*, **183**, 527–541, doi:10.1016/S0012-821X(00)00294-6.
- Long, M. D., and T. W. Becker (2010), Mantle dynamics and seismic anisotropy, *Earth Planet. Sci. Lett.*, **297**, 341–354, doi:10.1016/j.epsl.2010.06.036.
- Long, M. D., and P. G. Silver (2008), The subduction zone flow field from seismic anisotropy: A global view, *Science*, **319**, 315–318, doi:10.1126/science.1150809.
- Long, M. D., and R. D. van der Hilst (2006), Shear wave splitting from local events beneath the Ryukyu arc: Trench-parallel anisotropy in the mantle wedge, *Phys. Earth Planet. Inter.*, **155**, 300–312, doi:10.1016/j.pepi.2006.01.003.
- Miller, M. S., B. L. N. Kennett, and A. Gorbato (2006), Morphology of the distorted subducted Pacific slab beneath the Hokkaido corner, Japan, *Phys. Earth Planet. Inter.*, **156**, 1–11, doi:10.1016/j.pepi.2006.01.007.
- Nagaya, M., H. Oda, and T. Kamimoto (2011), Regional variation in shear-wave polarization anisotropy of the crust in southwest Japan as estimated by splitting analysis of Ps-converted waves on receiver functions, *Phys. Earth Planet. Inter.*, **187**, 56–65, doi:10.1016/j.pepi.2011.04.016.
- Nakajima, J., and A. Hasegawa (2004), Shear-wave polarization anisotropy and subduction-induced flow in the mantle wedge of northern Japan, *Earth Planet. Sci. Lett.*, **225**, 365–377, doi:10.1016/j.epsl.2004.06.011.
- Nakajima, J., T. Matsuzawa, A. Hasegawa, and D. Zhao (2001), Three-dimensional structure of Vp, Vs, and Vp/Vs beneath northeastern Japan: Implications for arc magmatism and fluids, *J. Geophys. Res.*, **106**, 21,843–21,857, doi:10.1029/2000JB000008.
- Nakajima, J., Y. Takei, and A. Hasegawa (2005), Quantitative analysis of the inclined low-velocity zone in the mantle wedge of northeastern Japan: A systematic change of melt-filled pore shapes with depth and its implications for melt migration, *Earth Planet. Sci. Lett.*, **234**, 59–70, doi:10.1016/j.epsl.2005.02.033.
- Nakajima, J., J. Shimizu, S. Hori, and A. Hasegawa (2006), Shear-wave splitting beneath the southwestern Kurile arc and northeastern Japan arc: A new insight into mantle return flow, *Geophys. Res. Lett.*, **33**, L05305, doi:10.1029/2005GL025053.
- Nikulin, A., V. Levin, and J. Park (2009), Receiver function study of the Cascadia megathrust: Evidence for localized serpentinization, *Geochem. Geophys. Geosyst.*, **10**, Q07004, doi:10.1029/2009GC002376.
- Nikulin, A., V. Levin, M. Carr, C. Herzberg, and M. West (2012), Evidence for two upper mantle sources driving volcanism in Central Kamchatka, *Earth Planet. Sci. Lett.*, **321–322**, 14–19, doi:10.1016/j.epsl.2011.12.039.
- Niu, F., A. Levander, S. Ham, and M. Obayashi (2005), Mapping the subducting Pacific slab beneath southwest Japan with Hi-net receiver functions, *Earth Planet. Sci. Lett.*, **239**, 9–17, doi:10.1016/j.epsl.2005.08.009.
- Park, J., and V. Levin (2000), Receiver functions from multiple-taper spectral correlation estimates, *Bull. Seismol. Soc. Am.*, **90**, 1507–1520, doi:10.1785/0119990122.
- Park, J., V. Levin, M. T. Brandon, J. M. Lees, V. Peyton, E. Gordeev, and A. Ozerov (2002), Dangling slab, amplified arc volcanism, mantle flow and seismic anisotropy in the Kamchatka plate corner, in *Plate Boundary Zones, Geodyn. Ser.*, vol. 30, edited by S. Stein and J. T. Freymueller, pp. 295–324, AGU, Washington, D. C., doi:10.1029/GD030p0295.
- Park, J., H. Yuan, and V. Levin (2004), Subduction-zone anisotropy under Corvallis, Oregon: A serpentinite skidmark of trench-parallel terrane migration?, *J. Geophys. Res.*, **109**, B10306, doi:10.1029/2003JB002718.
- Porter, R., G. Zandt, and N. McQuarrie (2011), Pervasive lower-crustal seismic anisotropy in Southern California: Evidence for underplated schists and active tectonics, *Lithosphere*, **3**, 201–220, doi:10.1130/L126.1.
- Ramesh, D. S., H. Kawakatsu, S. Watada, and X. Yuan (2005), Receiver function images of the central Chugoku region in the Japanese islands using Hi-net data, *Earth Planets Space*, **57**, 271–280.
- Salah, M. K., T. Seno, and T. Iidaka (2008), Upper mantle anisotropy beneath central and southwest Japan: An insight into subduction-induced mantle flow, *J. Geodyn.*, **46**, 21–37, doi:10.1016/j.jog.2008.04.002.
- Salah, M. K., T. Seno, and T. Iidaka (2009), Seismic anisotropy in the wedge above the Philippine Sea slab beneath



- Kanto and southwest Japan derived from shear wave splitting, *J. Asian Earth Sci.*, *34*, 61–75, doi:10.1016/j.jseae.2008.04.004.
- Savage, M. K. (1998), Lower crustal anisotropy or dipping boundaries? Effects on receiver functions and a case study in New Zealand, *J. Geophys. Res.*, *103*, 15,069–15,087, doi:10.1029/98JB00795.
- Savage, M. K., J. Park, and H. Todd (2007), Velocity and anisotropy structure at the Hikurangi subduction margin, New Zealand from receiver functions, *Geophys. J. Int.*, *168*, 1034–1050, doi:10.1111/j.1365-246X.2006.03086.x.
- Shiomi, K., and J. Park (2008), Structural features of the subducting slab beneath the Kii Peninsula, central Japan: Seismic evidence of slab segmentation, dehydration, and anisotropy, *J. Geophys. Res.*, *113*, B10318, doi:10.1029/2007JB005535.
- Shiomi, K., H. Sato, K. Obara, and M. Ohtake (2004), Configuration of subducting Philippine Sea plate beneath southwest Japan revealed from receiver function analysis based on the multivariate autoregressive model, *J. Geophys. Res.*, *109*, B04308, doi:10.1029/2003JB002774.
- Siebert, L., and T. Simkin (2002), Volcanoes of the world: An illustrated catalog of Holocene volcanoes and their eruptions, *Global Volcanism Program Digital Inf. Ser., GVP-3*, Smithsonian Inst., Washington, D. C. [Available at <http://www.volcano.si.edu/world/>.]
- Silver, P. G. (1996), Seismic anisotropy beneath the continents: Probing the depths of geology, *Annu. Rev. Earth Planet. Sci.*, *24*, 385–432, doi:10.1146/annurev.earth.24.1.385.
- Syracuse, E. M., and G. A. Abers (2006), Global compilation of variations in slab depth beneath arc volcanoes and implications, *Geochem. Geophys. Geosyst.*, *7*, Q05017, doi:10.1029/2005GC001045.
- Taira, A. (2001), Tectonic evolution of the Japanese island arc system, *Annu. Rev. Earth Planet. Sci.*, *29*, 109–134, doi:10.1146/annurev.earth.29.1.109.
- Tonegawa, T., K. Hirahara, T. Shibutani, and N. Fujii (2006), Lower slab boundary in the Japan subduction zone, *Earth Planet. Sci. Lett.*, *247*, 101–107, doi:10.1016/j.epsl.2006.04.036.
- Ulmer, P., and U. Trommsdorff (1995), Serpentine stability to mantle depths and subduction-related magmatism, *Science*, *268*, 858–861, doi:10.1126/science.268.5212.858.
- Wang, J., and D. Zhao (2008), P wave anisotropic tomography beneath Northeast Japan, *Phys. Earth Planet. Inter.*, *170*, 115–133, doi:10.1016/j.pepi.2008.07.042.
- Wang, J., and D. Zhao (2009), P wave anisotropic tomography of the crust and upper mantle under Hokkaido, Japan, *Tectonophysics*, *469*, 137–149, doi:10.1016/j.tecto.2009.02.005.
- Watanabe, T., H. Kasami, and S. Ohshima (2007), Compressional and shear wave velocities of serpentinized peridotites up to 200 MPa, *Earth Planets Space*, *59*, 233–244.
- Wessel, P., and W. H. F. Smith (1991), Free software helps map and display data, *Eos Trans. AGU*, *72*(41), 441, doi:10.1029/90EO00319.
- Wirth, E., and M. D. Long (2010), Frequency-dependent shear wave splitting beneath the Japan and Izu-Bonin subduction zones, *Phys. Earth Planet. Inter.*, *181*, 141–154, doi:10.1016/j.pepi.2010.05.006.
- Yamauchi, M., K. Hirahara, and T. Shibutani (2003), High resolution receiver function imaging of the seismic velocity discontinuities in the crust and uppermost mantle beneath southwest Japan, *Earth Planets Space*, *55*, 59–64.
- Yoshizawa, K., K. Miyake, and K. Yomogide (2010), 3D upper mantle structure beneath Japan and its surrounding region from inter-station dispersion measurements of surface waves, *Phys. Earth Planet. Inter.*, *183*, 4–19, doi:10.1016/j.pepi.2010.02.012.
- Zhao, D., Z. Wang, N. Umino, and A. Hasegawa (2009), Mapping the mantle wedge and interplate thrust zone of the northeast Japan arc, *Tectonophysics*, *467*, 89–106, doi:10.1016/j.tecto.2008.12.017.